



Modification of low-salt myofibrillar protein using combined ultrasound pre-treatment and konjac glucomannan for improving gelling properties: Intermolecular interaction and filling effect

Yongfang Gao^{a,b,c}, Yunpeng Hu^a, Jiakuan Wang^a, Hafiz Nabeel Ahmad^a, Jie Zhu^{a,b,c,*}

^a Laboratory of Agricultural and Food Biophysics, Institute of Biophysics, College of Science, Northwest A&F University, Yangling, Shaanxi 712100, China

^b Laboratory of Muscle Biology and Meat Science, National Beef Cattle Improvement Center, College of Animal Science and Technology, Northwest A&F University, Yangling, Shaanxi 712100, China

^c Laboratory of Meat Quality Analysis and Products Development, Ningxia Xihaigu Institute of High-end Cattle Industry, Haiyuan Hairun Agricultural Company, Haiyuan, Ningxia 755299, China

ARTICLE INFO

Keywords:

Myofibrillar protein
Konjac glucomannan
Ultrasound
Atomic force microscopy
Salt reduction

ABSTRACT

The quality deterioration of low-salt meat products has been gained ongoing focus of researchers. In this study, konjac glucomannan (KGM) was used to alleviate the finiteness of ultrasound treatment on the quality improvement of low-salt myofibrillar protein (MP), and the modification sequence was also investigated. The results revealed that the single and double sequential modification by utilizing KGM and ultrasound significantly influenced the gelation behavior of low-salt MPs. The uniform MP-KGM mixture formed by a single ultrasound treatment had limited protein unfolding, resulting in relatively weak intermolecular forces in the composite gel. Importantly, ultrasound pre-treatment combined with KGM modification promoted the unfolding and moderate thermal aggregation of proteins and remarkably improved the rheological behaviors and gel strength of the composite gel. This result could also be corroborated by the highest percentage of *trans-gauche-trans* conformation of S—S bridges and maximum β -sheet proportion. Furthermore, molecular dynamic simulation and molecular docking elucidated that the hydrogen bond length between protein and KGM was shortened after ultrasound pre-treatment, which was the molecular basis for the enhanced intermolecular interactions. Therefore, ultrasound pre-treatment combined with KGM can effectively improve the gelling properties of low-salt MPs, providing a practical method for the processing of low-salt meat products.

1. Introduction

Myofibrillar protein (MP), accounting for nearly 60 % of skeletal muscle protein, is the main functional-related protein that acts a dominant role in the gelation and textural properties of meat products [1]. Generally, salt-soluble MP exhibits an aggregation state at low salt concentrations (<0.3 mol/L), which causes alteration in protein conformation and deteriorates the quality of meat products [2]. However, excessive consumption of dietary salt has been linked to increased occurrence of stroke and hypertension [3]. Based on the detrimental effects of excessive sodium intake on human health, the research and development of high-quality low-salt meat products are imperative.

Regarding the increasing demand for healthier meat products with reduced sodium content, various strategies have been applied to

improve the performance of low-salt meat products, such as NaCl substitutes, plant proteins, polysaccharides [4], and alternative processing techniques [5]. Ultrasound has been widely applied in the food processing industry as an auxiliary means due to its cavitation effect [6]. Ultrasonic treatment could improve protein solubility and drive conformational changes of protein. Moderate ultrasonic treatment (≤ 300 W) has been reported to produce dense and uniform gel accompanied by enhanced water-holding capacity [7]. The underlying mechanisms mainly include ultrasound can effectively increase protein solubility, inhibit protein aggregation, and alter protein conformation. Nevertheless, excessive ultrasonic treatment resulted in serious protein denaturation and irregular gel structure [8], which limited the application of ultrasonic treatment in improving protein functional properties under low salt conditions. Consequently, studies to further improve the

* Corresponding author at: Laboratory of Agricultural and Food Biophysics, Institute of Biophysics, College of Science, Northwest A&F University, Yangling, Shaanxi 712100, China.

E-mail address: [jiezhu@nwafu.edu.cn](mailto:jiezhunwafu.edu.cn) (J. Zhu).

<https://doi.org/10.1016/j.ijbiomac.2023.126195>

Received 22 June 2023; Received in revised form 4 August 2023; Accepted 5 August 2023

Available online 7 August 2023

0141-8130/© 2023 Elsevier B.V. All rights reserved.

properties of single ultrasound-treated low-salt MP by incorporating functional substances are essential to explore the interactions between sample components that are closely related to matrix properties during gelation [9].

Plant polysaccharides are usually used to improve the water-retaining and gelling properties of processed meat products. Konjac glucomannan (KGM) is a neutral and water-soluble dietary fiber, which is primarily comprised of D-mannose and D-glucose linked through β -1,4-glycosidic bonds at a molar ratio of 1.6:1. Regarding the excellent water-holding capability and filling effect, previous studies showed that KGM could enhance the gelling properties of inferior squid surimi gel [10]. Notably, Zhuang and coauthors discovered that only a small amount of KGM addition ($\leq 1\%$) promoted the unfolding of MPs and the formation of compact gel matrix, however, excessive KGM addition ($> 1\%$) could form continuous hydrogel thereby weakening protein gel network and hindering the aggregation of MPs during thermal gelling process [11]. These results indicated that appropriate KGM addition could not only improve the gelling capacity of protein at high salt conditions (0.6 M NaCl) through filling effect but also be a functional component to alter protein conformation. In addition, our previous study found that KGM ($\leq 0.75\%$) could improve the gelling properties of the low-salt MP (0.3 M NaCl) by altering protein conformation [12], which was essential for developing low-salt meat products. As previously mentioned, ultrasound and KGM treatment might affect the physicochemical characteristics of proteins in different ways, thereby changing protein functional properties. Therefore, we hypothesized that the combination of ultrasound and KGM might synergistically improve the gelling properties of low-salt MPs, but the synergistic mechanism needs to be further explored. In addition, there is little intrinsic knowledge concerning the effect of different modification sequences on the characteristics of low-salt MP, which is crucial for the final qualitative properties of low-salt processed meat products. Analogously, previous research reported that ultrasound decreased the interaction strength between β -Lactoglobulin and sodium alginate, which may be beneficial or detrimental in relation to a particular functionality [13]. Regrettably, this field has been neglected in recent researches [14].

In the current study, we investigated the mechanisms underlying the effects of different modification sequences of KGM and ultrasound on the conformational and gelling behavior of low-salt MP molecules. The results are expected to broaden the practical application of KGM and ultrasound treatment in healthy low-salt meat products.

2. Materials and methods

2.1. Materials and chemicals

Fresh *Longissimus dorsi* muscle was obtained from seven Qinchuan cattle slaughtered at the Yangling Kangle Market (Shaanxi, China). Muscle chunks (~ 25 g) were stored at -80°C for the extraction of myofibrillar protein. Konjac glucomannan (CAS: 37220-17-0) was acquired from Solarbio Co., Ltd. (Beijing, China).

2.2. Extraction of myofibrillar protein

Frozen muscle chunks were thawed at 4°C for 1 h, and then myofibrillar protein was extracted according to the method previously depicted in detail by Wang and his colleagues [8]. The Biuret method was used to assess protein concentration, and the protein precipitate was held on an ice slurry and used within 12 h.

2.3. Sequential modification of MPs through KGM and ultrasonic treatment

MP isolate was dispersed in 20 mM phosphate buffer (pH 7.4, 0.3 M NaCl) containing KGM (0.75 g/100 g MP) to a final protein concentration of 30 mg/mL and incubated at 4°C for 12 h (MP-KGM). The KGM

concentration was determined based on previous investigation [12]. MP sample (25 mg/mL) was ultrasonicated in a probe-type ultrasonic processor (JY 92-IIN, Ningbo, China) for 8 min (frequency 20 kHz; amplitude 28 %; power 250 W; on-time 1 s and off-time 2 s) and the temperature was maintained below 8°C using an ice bath. The corresponding ultrasound intensity was $10.25 \pm 0.24\text{ W/cm}^2$ as measured referring to the previous method [15]. The dual modification of low-salt MP by KGM and ultrasonic treatment was assigned to the following two groups: the ultrasonicated MP was mixed with KGM ($U_{\text{MP-KGM}}$), and the MP and KGM were mixed for sonication ($U_{\text{MP-KGM}}$). Non-treated MP samples were prepared as the control.

2.4. Structural characteristics of MPs

2.4.1. Intrinsic tryptophan fluorescence

The fluorescence intensity of MP suspension (0.2 mg/mL dissolved in 20 mM phosphate buffer) was measured using an LS55 spectrofluorometer (Shanghai Simiao Analytical Instrument, Shanghai, China), as previously described by Jiang and his colleagues [16]. The protein emission spectra were obtained under an excitation wavelength of 280 nm.

2.4.2. Surface hydrophobicity

The hydrophobic groups of different treated MPs were determined using a hydrophobic probe of Bromophenol Blue [17]. 200 μL of BPB probe (1 mg/mL) was added to aliquots of protein suspension (1 mL, 5 mg/mL) and incubated for 30 min. Subsequently, the mixture was centrifuged at $4000 \times g$ for 10 min using a refrigerated centrifuge (KDC-160HR, Zhongke Zhongjia Co., Ltd). The UV absorbance of diluted supernatant ($10\times$) was obtained at 595 nm (A_{sample}) using a spectrophotometer (P5, Mapada Instruments Co., Shanghai, China). The phosphate buffer was used to determine the absorbance of the blank (A_{control}). The protein hydrophobicity was calculated through Eq. (1).

$$\text{BPB bound } (\mu\text{g}) = 200 \times (A_{\text{control}} - A_{\text{sample}}) / A_{\text{control}} \quad (1)$$

2.4.3. Far-ultraviolet circular dichroism spectroscopy (CD)

The secondary structure of protein samples was explored using the ChirascanTM spectrometer (V100, Applied Photophysics Ltd., England). The MP suspension was transferred to a quartz cuvette. The molar ellipticity in millidegrees (mdeg) was measured under a scan rate of 50 nm/min. The content of each secondary structure (α -helix, β -sheet, β -turn, random coil) was analyzed using the DichroWeb site [18]. All protein samples were scanned three times to obtain the average value.

2.5. Protein profile and solubility

The protein cross-linking and polymerization in MP suspensions and heat-induced gels were examined according to the previous study [1]. In this study, β -Mercaptoethanol (β -ME) was utilized to sever disulfide bridges (S—S). Protein solubility (%) was calculated as the protein concentration ratio of supernatant obtained by centrifugation (4°C , $5000 \times g$, 15 min) and original suspension (5 mg/mL).

2.6. Emulsifying properties of MPs

2.6.1. Emulsifying activity (EA) and emulsion stability index (ESI)

Protein emulsion was obtained by mixing 4 mL of MP suspension (10 mg/mL) with soybean oil (1 mL) and homogenized at 11000 rpm for 60 s using a homogenizer (IKA, Germany). Subsequently, 40 μL of protein emulsion was obtained at the bottom and diluted to 4 mL with SDS solution (1 mg/mL). The absorbance of the diluted protein emulsion was determined immediately (A_0) or after 10 min (A_{10}) at 500 nm. The EA and ESI of MPs were calculated according to the Eqs. (2) and (3).

$$EA \text{ (m}^2/\text{g)} = \frac{2.303 \times 2 \times A_0 \times D}{C \times F \times 10,000} \quad (2)$$

$$ESI \text{ (%) } = \frac{A_0}{(A_0 - A_{10})} \times 100\% \quad (3)$$

where A_0 and A_{10} represent the UV absorbance at 0 and 10 min, D is the dilution ratio, C represents MP concentration (g/mL), and F represents the volume fraction of soybean oil (20 %).

2.6.2. Fluorescence microscope observation

Fluorescence microscope (DM5000 B, Leica Microsystem GmbH, Germany) was applied to observe the microstructure of emulsions at 10-fold magnification. Nile Red solution (100 μ L, 0.1 % in ethanol) and fluorescein isothiocyanate solution (FITC, 100 μ L, 0.01 % in acetone) were added to protein emulsion and then stored in the dark for 40 min. The stained MP emulsion (50 μ L) was viewed on a microscope slide, and the excitation wavelength of Nile Red and FITC were 488 nm and 552 nm, respectively.

2.7. Atomic force microscopy imaging of MPs and MP aggregates

The nanomorphology of protein samples was analyzed with Multimode-8 atomic force microscopy with SCANASYST-AIR probes (Bruker Co., Billerica, MA, USA) according to the previous approach [19]. Topography of MP suspension: the 10 μ L of MP solution (15 μ g/mL) was dropped onto a mica sheet and deposited in the air for 3 h. The observation of MP thermal aggregates: 10 μ L of heated MP suspension (10 μ g/mL, 75 $^{\circ}$ C for 20 min) was scanned as above steps. The image analysis was carried out using Nanoscope Analysis V1.10 offline software (Billerica, MA, USA), which was applied specifically for the determination of the height, diameter, and image roughness (R_q) of samples. Each sample was scanned at least in triplicate, and the average value was analyzed. Image R_q was calculated according to Eq. (4) as follows.

$$R_q = \sqrt{\int_0^l Z^2(x) dx / l} \quad (4)$$

where $Z(x)$ is the ordinate value, l represents the sampling length.

2.8. The rheological properties of MP sols

The rheological properties of protein suspensions (25 mg/mL) were measured using a DHR-1 rheometer (TA Instruments, USA) according to a published method [20]. Degassed protein suspension (1.5 mL) was transferred to the plate and sealed with silicone oil. After equilibrating between two parallel plates for 180 s, protein suspension was sheared (0.1 to 100 s^{-1}) to record the viscosity. In addition, protein suspensions were heated from 20 to 75 $^{\circ}$ C to determine the modulus (G' , G''). The strain sweep was performed to determine the linear region of MP solutions at 0.1 Hz before testing.

2.9. Preparation of MP gels

Protein gels were obtained by pouring 15 mL of 25 mg/mL protein sol into glass beakers and heated from 23 $^{\circ}$ C to 75 $^{\circ}$ C to induce complete gelation. After gelation, protein gels were quickly put on the ice slurry for 10 min and stored in the 4 $^{\circ}$ C refrigerator.

2.10. Gelling properties of MPs

2.10.1. Water holding capacity (WHC) and cooking loss

The WHC of MP gels was determined by calculating the weight percentage of the centrifuged (3500 \times g, 20 min) gel to the initial gel. Cooking loss was calculated as the weight ratio of expelled liquid during

the thermal treatment to the original sol [1].

2.10.2. Gel strength and texture profile analysis

The gel strength was determined using a TA texture analyzer (Stable Micro System Co., London, U.K.) equipped with a P/0.5 probe (diameter of 12.7 mm). Subsequently, gel columns (21 \times 15 mm) were detected under specific parameters (trigger force, 5 g; pre-test and test speed, 1.0 mm/s; post-test speed, 3.0 mm/s). The gel strength was defined as the initial force required to break the gel matrix.

The texture profile analysis (TPA) of MP gels was measured using a texture analyzer with the P/0.5R probe. Protein gel was axially compressed to 50 % of their original height. The compressed interval, test speed and trigger force were set as 5 s, 1 mm/s, and 5 g separately.

2.10.3. Differential scanning calorimetry

The thermal characteristics of protein samples were investigated using a TA scanning calorimetry (New Castle, USA). A sealed empty plate was prepared as a reference. The freeze-dried protein sample (10 mg) was heated from 20 to 110 $^{\circ}$ C at 1 $^{\circ}$ C/min. The denaturation temperature of protein samples was obtained using Universal software.

2.10.4. Raman spectroscopy

Protein gels were scanned using DXR2 laser microscopic spectrometer (Austin, USA) equipped with a 10 \times /0.25 BD microscope, and the laser source was set at 785 nm. The gel samples were scanned 30 times under a laser power of 17 mW. The spectrogram was collected and subsequently analyzed to obtain the secondary structure and microenvironment of protein using the Omnic7.3 software.

2.10.5. Topological morphology of MP gels

MP suspension (20 μ L, 20 mg/mL) was dropped onto mica and heated in a water bath from 20 to 75 $^{\circ}$ C at a rate of 1 $^{\circ}$ C/min. Subsequently, samples were dried at room temperature (25 $^{\circ}$ C, 6 h) to form a protein layer. Deionized water was used to wash the superficial salt crystal. AFM height images (5.0 \times 5.0 μ m, $n \geq 6$) in 512 \times 512 pixels of each sample were obtained after a second-order flatten.

2.10.6. Confocal laser scanning microscopy

The specific distribution of MP and KGM in protein gels was evaluated using an CLSM (TCS SP8 SR, Germany). Gel pieces (2 \pm 0.5 mm in thickness) were stained with a mixed staining solution of 1 mL that contained 0.1 % (w/v) Rhodamine B and 0.1 % Calcofluor white for 40 min before being rinsed with distilled water to remove any surplus staining solution. The gel samples were analyzed using two laser channels and a 10 \times objective lens (channel 1: Calcofluor white, 405 nm; channel 2: Rhodamine B, 488 nm).

2.10.7. Molecular forces in MP gels

The protein gel (1 g) was homogenized with 9 mL of different liquids respectively, following the method previously outlined by Jiang et al. [21]. The five solutions used were as follows: 0.05 M NaCl (S1), 0.6 M NaCl (S2), 1.5 M urea + 0.6 M NaCl (S3), 8.0 M urea + 0.6 M NaCl (S4), and 8.0 M urea + 0.5 M β -mercaptoethanol + 0.6 M NaCl (S5). Sample homogenates were centrifuged at 8000 \times g for 20 min after being continuously agitated at 4 $^{\circ}$ C for 40 min. Protein concentration in above-mentioned supernatant was measured using the Biuret Method. The concentration differences between S2 and S1, S3 and S2, S4 and S3, and S5 and S4 represent the content of ionic bonds, hydrogen bonds, hydrophobic interactions, and disulfide bonds separately.

2.11. Molecular dynamics simulation

The protein used in the dynamic simulation was obtained from UniProtKB (<https://www.UniProt.org/>), and the genebank accession number was E1BPK6. The simulation process was conducted in a water-cubic box (12 nm \times 18 nm \times 18 nm) with periodic boundary conditions

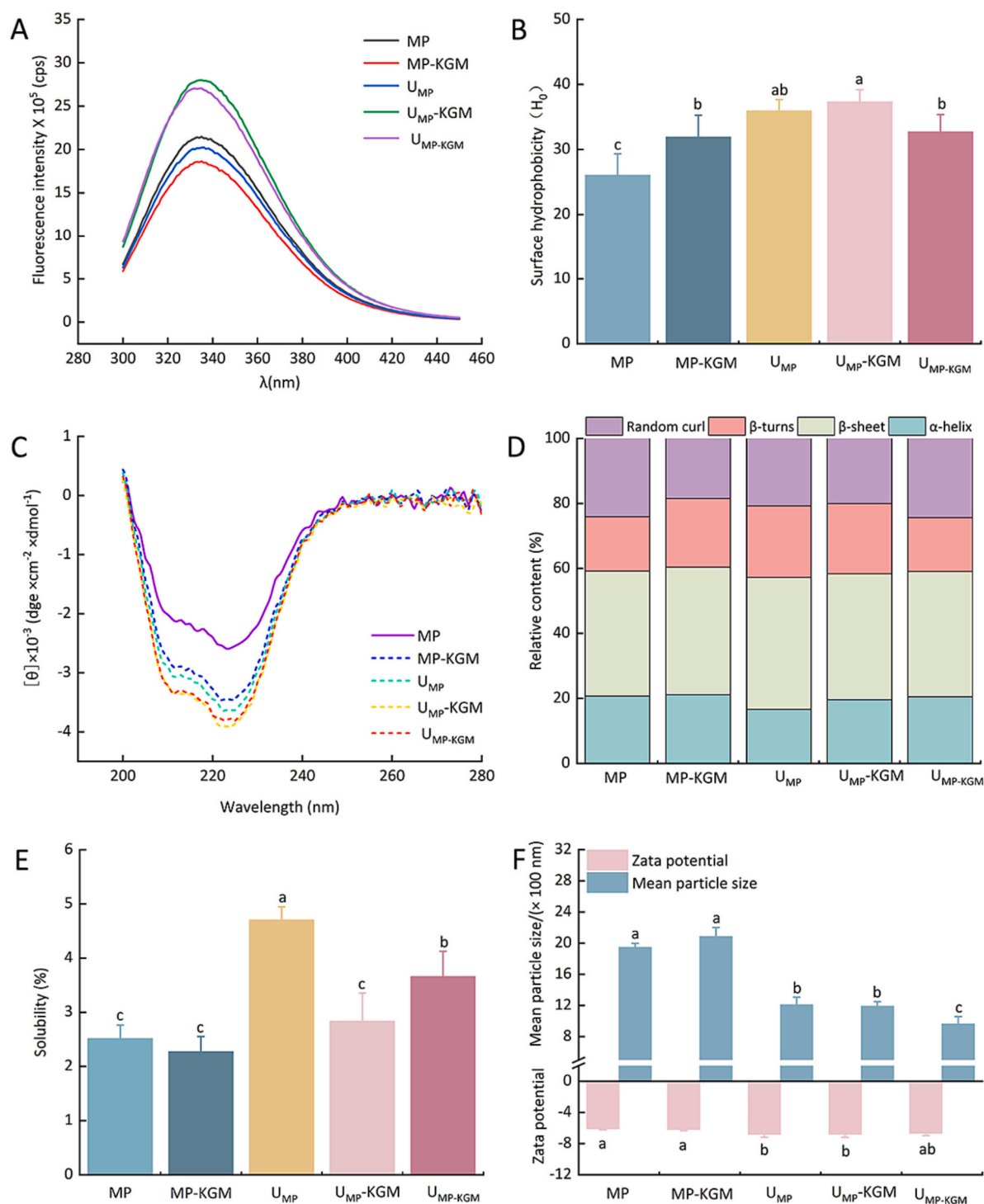


Fig. 1. Changes in myofibrillar protein (MP) properties. Fluorescence intensity (A), surface hydrophobicity (B), circular dichroic spectra (C), secondary structure proportion (D), solubility (E), mean particle size and zeta potential (F) of MP samples. Error bars indicate the standard errors of the mean. Different lowercase letters represent significant differences ($P < 0.05$).

to maintain a constant number of particles. The simulated system was subjected to 5000-step energy minimization. After energy minimization, a 100 ps simulation was performed under NVT (the constant Number of particles, Temperature and Volume) and NPT (the constant Number of particles, Temperature and Pressure) conditions. The cut-off distance for non-bonding interaction was set to 12 Å. The long-range electrostatic force was calculated using the Particle Mesh Ewald (PME) summation method. By utilizing V-rescale, the temperature was maintained at 281 K with a coupling constant of 0.1 ps. The whole model system was

simulated for 100 ns, and the data analysis was conducted using simulation trajectory files.

2.12. Molecular docking of myofibrillar protein and KGM

The interaction between KGM (Compound CID: 24892726) and myosin (the main component of myofibrillar protein) was predicted using the Autodock Vina 1.1.2 software, and the docking conformation was set to 10. The conformation with the largest absolute value of

binding energy value was selected as the docking result, and the Discovery Studio 2019 Client was used for visualization.

2.13. Statistical analysis

After three independent repetitions, all data were shown in the form of mean \pm standard deviations. The variance analysis was evaluated using SPSS 26.0 software. The significance of differences in mean values was evaluated using a one-way analysis of variance (ANOVA) and the Duncan multiple tests ($P < 0.05$).

3. Results and discussions

3.1. Structural characteristics of MPs

3.1.1. Tryptophan fluorescence of proteins

The tryptophan residues on proteins are typically used to monitor conformational changes of proteins due to their sensibility to the local microenvironment. As illustrated in Fig. 1A, the highest fluorescence emission from the pure low-salt MP peaked at 335 nm, which was similar with the earlier observation [22]. It is generally reported that partially or completely unfolded proteins would see a fall in fluorescence intensity, while folded proteins show a higher fluorescence intensity. Ultrasonic treatment significantly reduced the fluorescence intensity of low-salt MP, accompanied with a mild red shift (1 nm) in the wavelength of maximum emission (λ_{\max}), demonstrating that the tryptophan residues were exposed to a more hydrophilic environment and that the protein was outspread. Compared to pure low-salt MP, KGM modification caused a decrease in fluorescence intensity specifically. Zhuang and his colleagues reported a similar phenomenon in pork ham MP incubated with KGM, attributing the reduction of fluorescence intensity to the specific modification of tryptophan residues [11]. However, KGM modification combined with ultrasonic treatment (U_{MP-KGM} , U_{MP-KGM}), regardless of the modification sequence, caused a substantial increase in the fluorescence intensity ($P < 0.05$) compared to pure low-salt MP. As mentioned before, the conceivable noncovalent modification between KGM and tryptophan residues led to the unfolding of MP [11]. For the U_{MP-KGM} group in which ultrasound was carried out before KGM addition, ultrasonic pretreatment already promoted the expansion of low-salt MP [23]. Therefore, the hydrophilic KGM might coat on the surface of MP particles and form a polysaccharide layer around protein molecules, which suggested that the unfolding effect of KGM had mostly been exterminated, thereby shielding certain fluorescence signals [24]. The enhanced fluorescence intensity of the U_{MP-KGM} group in which KGM addition was carried out prior to the ultrasonic treatment might be due to the unfolding of non-covalent bonds between MP and KGM after ultrasound treatment, which causes the expansion of protein molecules and the appearance of a uniform soluble complex system [25], which may allow tryptophan residues to be uniformly buried within the protein structure.

3.1.2. Surface hydrophobicity of proteins

The hydrophobicity of protein surface may reflect the exposure of hydrophobic groups inside protein molecules and characterize protein conformational changes. As presented in Fig. 1B, the hydrophobicity of low-salt MPs increased significantly after KGM modification or ultrasonic treatment in all groups, suggesting the exposure of hydrophobic residues. As a result, more BPB could bind with the previously masked hydrophobic groups inside protein molecules. Analogously, Chen and his colleagues found that ultrasonic treatment induced the unfolding of chicken protein, resulting in the transfer of hydrophobic regions to protein surface [20]. In addition, surface hydrophobicity is associated with regions on the protein surface that are most likely to interact with binding ligands. Compared with KGM modification (MP-KGM), the higher hydrophobicity of low-salt MP after ultrasonic treatment (U_{MP}) indicated stronger hydrophobic interaction between protein molecules.

The hydrophobicity increased significantly for the dual-modified low-salt MP in which ultrasound was carried out before KGM addition (U_{MP-KGM}). The reason for such behavior might be that the cavitation effects induced by ultrasonic treatment might fragment low-salt MP particles and reduce MP aggregation, which facilitated low-salt MP and KGM intermolecular interaction, implying the synergistic effect of ultrasonic pretreatment and subsequent KGM modification. For the U_{MP-KGM} sample in which KGM addition was carried out prior to the ultrasonic treatment, the hydrophobicity appeared a decline compared with U_{MP} and U_{MP-KGM} groups. For U_{MP-KGM} protein, the homogenization of low-salt MPs was caused by ultrasound after the attachment of KGM, which might allow a greater number of KGM molecules to attach on the surface of protein particles and promote the uniformity of mixed suspension, thereby slightly hindering the exposure of hydrophobic “patches”.

3.1.3. Secondary structure of MPs

The secondary structure changes of proteins can be investigated using the far ultraviolet CD spectrum. As shown in Fig. 1C, two negative peaks appeared at 208 and 222 nm, which represent the superhelix conformation of myosin tail. Specifically, variations in the secondary structure of proteins correspond to changes in the intensity and shape of CD bands. The α -helix structure is mainly stabilized by the hydrogen bond between amino and carbonyl groups of the protein. Interestingly, the molar ellipticity of MP decreased after KGM or ultrasound treatment, which illustrated the reduction of spiral content [26]. This result also reflected a decrease in the structural compactness of MPs and the increase in the exposure of hydrophobic residues, which corresponds to the increased β -sheet proportion (Fig. 1D). Obviously, KGM and ultrasound modification induced the increase of β -sheet content at the price of α -helix structure, resulting in a more ductile and flexible structure of MPs. Importantly, the content of random coil in the U_{MP-KGM} group was markedly lower relative to that of ultrasound treated proteins, indicating the expansion of proteins, which was helpful for the development of the protein gel network [27].

3.2. Protein solubility and particle size

Solubility is an effective indicator of functional characteristics as a direct reflection of changes in aggregation, degradation and conformation of proteins [20]. As presented in Fig. 1C, low-salt MP solution treated with ultrasound had a considerably higher solubility than pure MP, which suggested the conformational alteration and the decreased MP aggregation caused by cavitation. Similar results have been found in the study of chicken actomyosin [23]. The decreased solubility of protein after KGM modification indicated a destabilization of the composite system with increased heterogeneity [28]. The U_{MP-KGM} sample existed a higher solubility as compared with U_{MP-KGM} protein, suggesting the formation of a more homogeneous system.

As shown in Fig. 1D, KGM modification significantly increased the particle size of MP in the mixed suspension as compared to control low-salt MP ($1.95 \pm 0.07 \mu\text{m}$), possibly due to that the interaction between hydrophilic KGM and protein molecules led to the union between low-salt MP and KGM. The same phenomenon was reported in chicken plasma protein solution added with KGM by Zou and his partners [25]. The size of protein particles in U_{MP} , U_{MP-KGM} and U_{MP-KGM} groups decreased significantly after ultrasonic treatment. The cavitation effect induced by ultrasound promoted the formation of soluble protein suspension, thus reducing the particle size of proteins. Compared with the MP in U_{MP-KGM} group, the lower particle size of MP in U_{MP-KGM} group indicated a stronger homogenization of the low-salt MP mixture.

3.3. ζ -Potential analysis

Zeta potential represents the surface charge of MP particles in the suspension, reflecting the dispersion or aggregation behavior of MP molecules in the solution. As seen in Fig. 1D, the zeta potential between

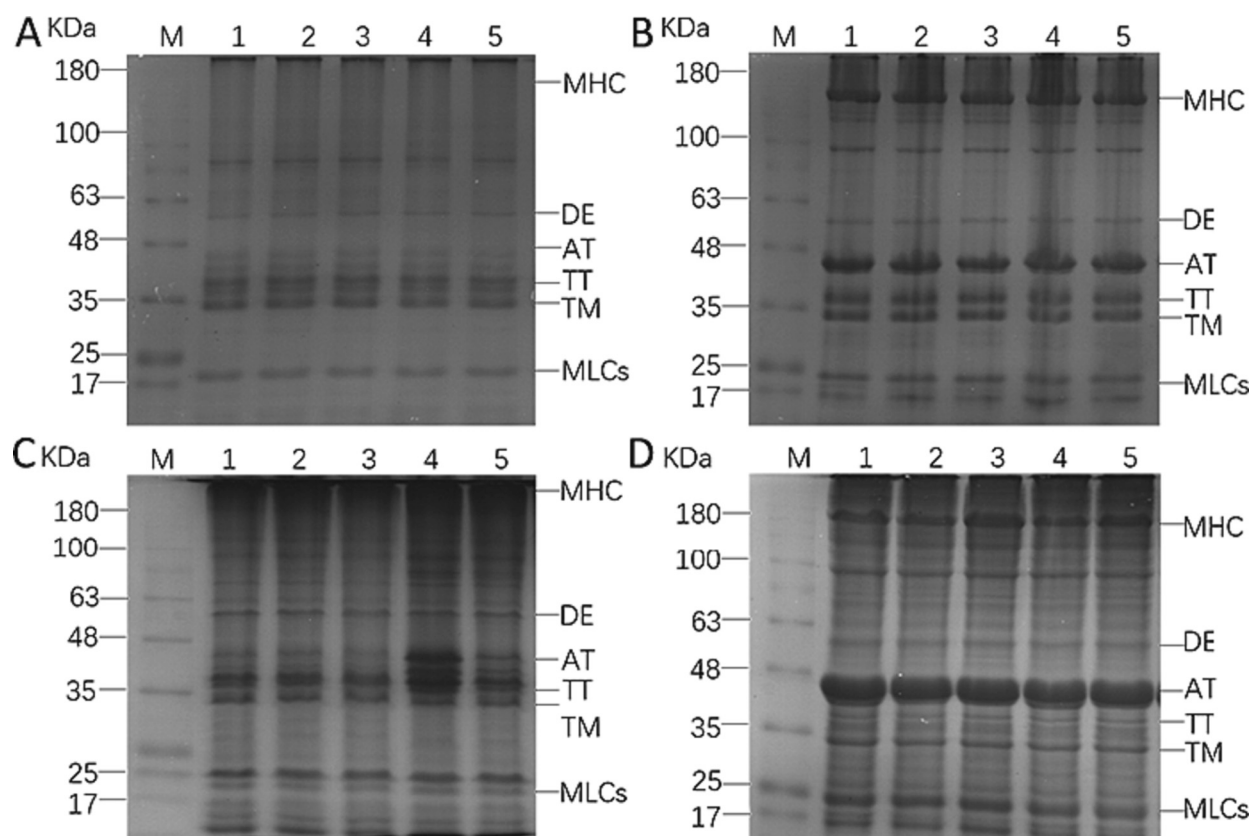


Fig. 2. Protein electrophoresis patterns of different treated MPs. SDS-PAGE patterns of MP suspensions without β -Me (A), MP suspensions with β -Me (B), MP gels without β -Me (C), and MP gels with β -Me (D). 1: MP, 2: MP-KGM, 3: U_{MP} , 4: U_{MP} -KGM, 5: U_{MP} -KGM. MW: protein standard. MHC: myosin heavy chain. DE: Desmin. AT: actin. TT: Troponin-T. TM: Tropomyosin. MLCs: myosin light chains.

the control and MP-KGM samples did not reveal any appreciable variations, mainly due to KGM is free of charge. Meanwhile, proteins in the U_{MP} , U_{MP} -KGM, and U_{MP} -KGM groups had higher absolute ζ -potential than the group of pure MP molecules. The enhancement in absolute ζ -potential of low-salt MP after ultrasonic treatment may be interpreted that ultrasonic treatment decomposed low-salt MPs into particles with smaller sizes, resulting in the enlargement in specific surface area of MP particles and the increase in the distribution of charges on the particle surface eventually (Zou et al., 2018). Specifically, the absolute ζ -potential of U_{MP} -KGM sample was slightly lower than that of U_{MP} and U_{MP} -KGM, which suggested that the exposure of charged groups was hampered by the homogeneous attachment of KGM molecules on the surface of protein particles.

3.4. MP profiles

The changes in protein patterns of low-salt MP suspensions (unheated, Fig. 2A-B) and heat-induced gels (Fig. 2C-D) under different modifications were observed using reducing and non-reducing electrophoresis. The characteristic fractions such as myosin heavy chain (MHC, ~200 kDa), actin (~42 kDa), Troponin-T (~37 kDa), tropomyosin (~35 kDa) and myosin light chains (MLC) were all detected in MP samples (Fig. 2), almost were identical to our previous findings [19]. The banding patterns of low-salt MPs were not appreciably impacted by KGM modification or ultrasonic treatment in the absence of -ME (Fig. 2A). In addition, the lost proteins, including MHC and actin, were mostly restored when the reducing agent β -ME was present (Fig. 2B), suggesting that the cross-linking between MPs was driven by disulfide linkages (S—S).

In the presence of β -ME, no significant difference between the control protein gel and modified protein gels was observed, as seen in Fig. 2D.

Additionally, as shown in Fig. 2C, the contents of myosin and actin fractions reduced in the absence of β -ME as compared with MP gels treated with β -ME, indicating the existence of disulfide bonds between actin and myosin in the protein gel, which was similar with the findings published by Xia and his collaborators [29]. The actin level in modified protein gels (MP-KGM, U_{MP}) was lower than that of control protein gel in the reducing condition, indicating that the development of disulfide bridges was promoted. Interestingly, samples of U_{MP} -KGM gel and U_{MP} -KGM gel exhibited new bands in the non-reducing condition, suggesting that dual modification might influence the formation and transformation of intramolecular and intermolecular S—S bridges.

3.5. Emulsifying characteristics of MPs

3.5.1. EA and ESI of MPs

The emulsifying activity refers to the adsorption capacity of protein particles at the water-oil interface to avoid gravity separation and flocculation of emulsions. As presented in Fig. S1A, KGM addition increased the emulsifying activity of MP as compared to pure protein. This might result from the enhanced exposure of hydrophobic sites (Fig. 1B), which facilitated the adhesion of MPs to the oil-water interface, resulting in a thicker protein adsorption layer. Analogously, *Artemisia sphaerocephala* Krasch gum improved the emulsifying activity of MP [30]. Moreover, the emulsifying capacity of MP significantly increased after ultrasound treatment (U_{MP} , U_{MP} -KGM, U_{MP} -KGM), presumably as a result of enhanced exposure of buried hydrophobic “patches” and the significant reduction in particle size caused by ultrasound cavitation and homogenization. The emulsion stability index (ESI) characterizes the ability of an emulsion to resist flocculation over a certain period. Consistent with changes in the emulsifying activity, the ESI of low-salt MPs modified by KGM or ultrasound treatment showed a

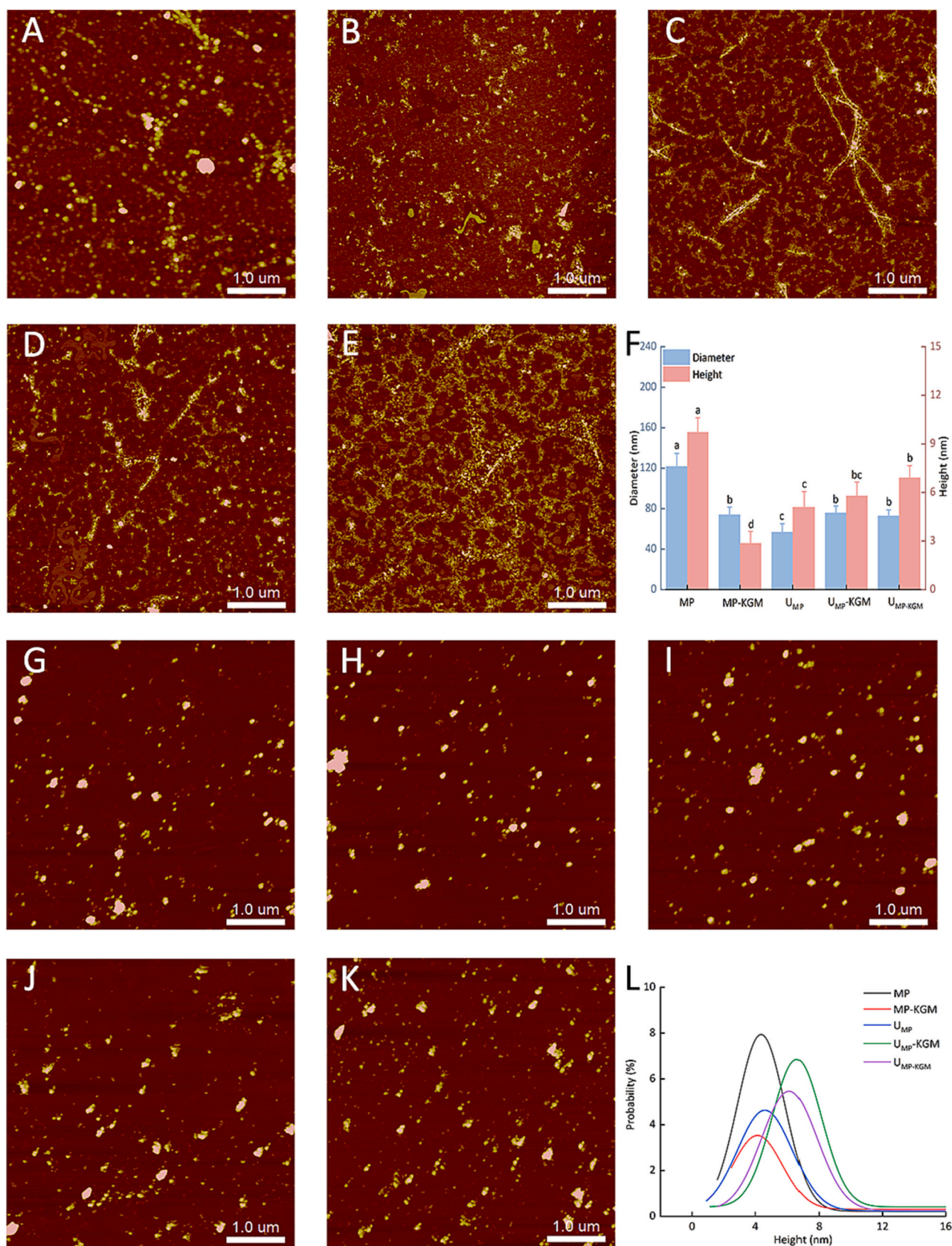


Fig. 3. Topography of MP particles (A-E) and MP thermal aggregates (G-K). Typical AFM height images of MP particles (A: MP, B: MP-KGM, C: U_{MP} , D: U_{MP} -KGM, E: U_{MP} -KGM) and the average height and diameter of MP particles obtained by particle analysis according to the corresponding AFM image (F). Thermal aggregation behavior of MP particles (G: MP, H: MP-KGM, I: U_{MP} , J: U_{MP} -KGM, K: U_{MP} -KGM) and the Gaussian distribution curves of the height of MP aggregates (L). Scale bar = 1 μ m. Different lowercase letters represent significant differences ($P < 0.05$).

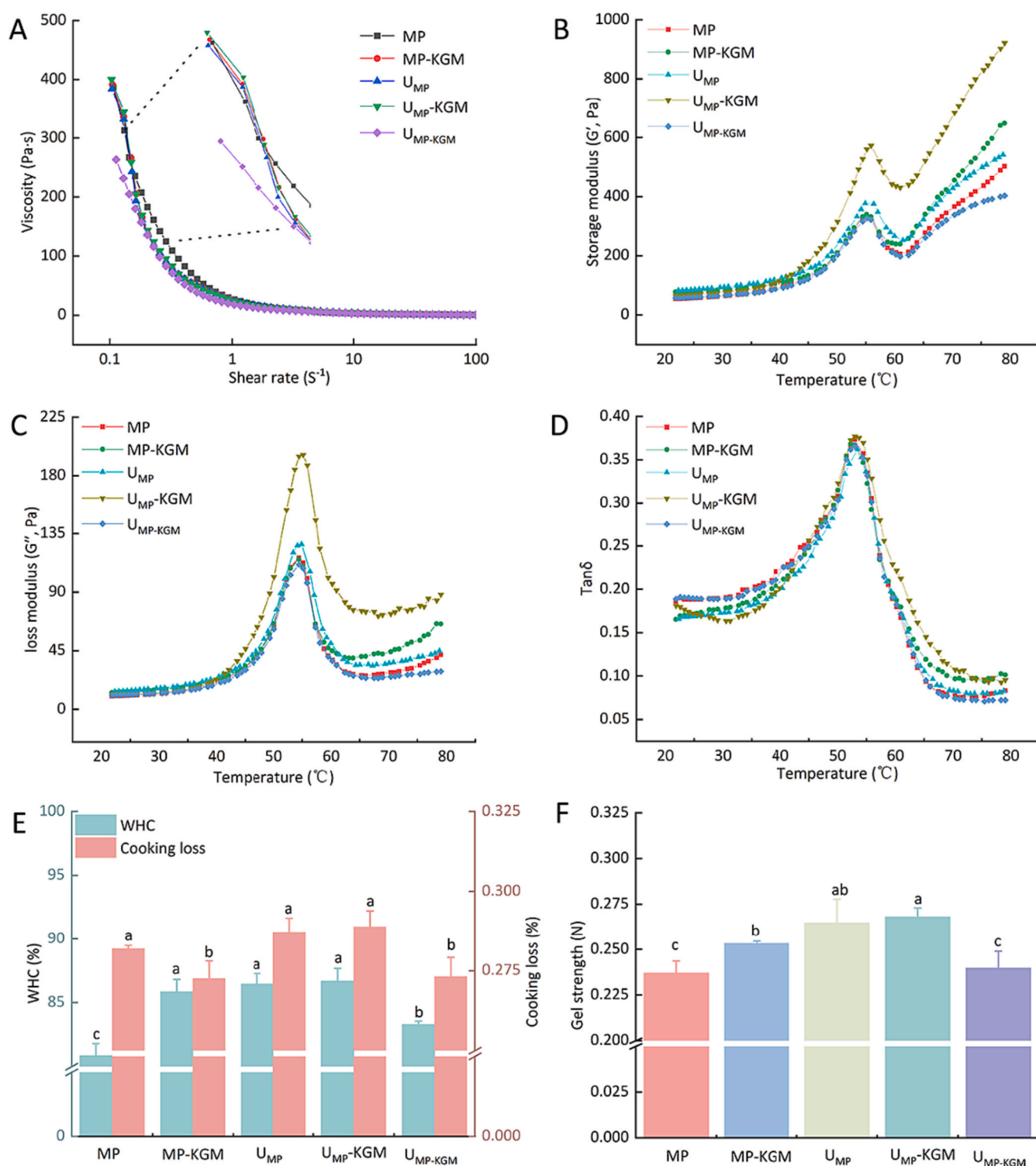


Fig. 4. Rheological properties of MP sols (A: apparent viscosity, B: storage modulus, C: loss modulus, D: loss tangent) and the gelation properties of MPs (E: water holding capacity (WHC) and cooking loss, F: gel strength). Error bars refer to the standard deviations. Different lowercase letters represent significant differences ($P < 0.05$).

similar increasing trend (Fig. S1B). Importantly, the U_{MP-KGM} sample existed optimum ESI value as compared with U_{MP} and U_{MP-KGM} groups, indicating that the uniform MP-KGM mixture obtained by ultrasound treatment could effectively maintain MP emulsion system. Hence, the uniform protein dispersion system induced by the ultrasonic cavitation effect mainly explains the excellent stability of U_{MP-KGM} emulsion.

3.5.2. The fluorescence staining observation of MP emulsion

To investigate the distribution of oil droplets and MP particles, the interfacial structure of MP emulsion was observed by fluorescence microscopy (Fig. S1). The micrographs in the upper row and lower row correspond to the distributions of oil droplets (dyed with Nile Red) and MPs (dyed with FITC), respectively. Obviously, the red oil droplets were surrounded with green MP layers, which could hinder the aggregation of

oil droplets. The protein boundary was weaker in the control protein, while the interfacial coverage was more pronounced in modified emulsions (MP-KGM, U_{MP} , U_{MP} -KGM, U_{MP} -KGM). Regarding abundant hydroxyl groups, previous studies showed that KGM might interact with protein molecules through non-covalent interactions [12], resulting in improved emulsion stability. Besides, the decreased size of oil droplets in ultrasound treated groups might be due to the enhanced interaction between MPs and oil droplets. Importantly, the emulsion droplet was uniform in the U_{MP} -KGM group, which was in line with the emulsion stability results (Fig. S1B).

3.6. Topography of MPs

The morphology of proteins was displayed in Fig. 3A-E. The pure low-salt MP exhibited a typical spherical distribution (diameter: 121.5 ± 13.09 nm, height: 9.72 ± 0.90 nm) and aggregated into long chains with the appearance of larger aggregates. KGM modification or ultrasonic treatment significantly altered the morphology of MPs. Compared with the control, KGM modification induced a more irregular or crude surface of MPs (diameter: 73.88 ± 7.67 nm, height: 2.87 ± 0.73 nm), which indicated that KGM could not contribute to a more continuous and homogeneous mixture. However, the protein molecules in the U_{MP} group showed a uniform crosslinking and fibrous assembly compared to the control group, which might be caused by protein unfolding and appropriate exposure of hydrophobic residues, hindering the formation of larger irregular MP aggregates. Similar results that shorter fibrils and fibrous assemblies were observed under moderate ultrasonic power (400 W), thereby improving protein solubility, which could be due to changes in surface hydrophobicity and electrostatic interactions induced by ultrasound. In addition, a uniform and dispersed morphology of MP particles was observed in U_{MP} -KGM group as compared to the U_{MP} -KGM group, which was consistent with the minimum protein particle size obtained in Fig. 1D.

3.7. Thermal aggregate behavior

Proteins may form polymers in response to heat stimulation. It could be seen that the pure low-salt MP aggregated to form a protein cluster, as shown in Fig. 3G. This finding was in accordance with the thermal aggregation behavior of pork myosin in Han's publication [31]. In addition, the crosslinking degree between protein clusters and the height of protein aggregates increased after KGM modification or ultrasonic treatment. The height histograms of AFM 2D images, as shown in Fig. 3L, were used to develop Gauss fit curves, which further confirmed these findings. The peak height of control protein aggregates was 4.37 ± 0.08 nm, which was lower than that in the group of U_{MP} (4.61 ± 0.11 nm), group of U_{MP} -KGM (6.60 ± 0.11 nm) and a group of U_{MP} -KGM (6.13 ± 0.09 nm), suggesting that the weak aggregation level of control protein and ultrasonic treatment promoted protein aggregation due to the cavitation effect [12]. Furthermore, the full width value at the maximum of pure protein aggregates (2.98 ± 0.17 nm) had increased to 3.11 ± 0.49 nm (MP-KGM), 3.45 ± 0.24 nm (U_{MP}), 3.09 ± 0.23 nm (U_{MP} -KGM), and 3.47 ± 0.18 nm (U_{MP} -KGM) separately. Accordingly, U_{MP} -KGM modification developed the appropriate aggregation of proteins and the uniform distribution of MP aggregates, which might yield a better gel structure.

3.8. Rheological properties

3.8.1. Flow properties

The apparent viscosity of protein sols revealed similar drops accompanied by a rise in the shear rate before stabilizing with no discernible difference, indicating the non-Newtonian shear-thinning behavior of all MPs. The initial viscosity of all treated protein suspensions except the U_{MP} and U_{MP} -KGM groups was higher than that of the control. Similar increased viscosity and shear thinning behavior were

also found in myofibrillar protein/sodium alginate mixtures, possibly due to the thickening effect of polysaccharides [4]. Higher apparent viscosity usually means lower fluidity, which might be caused by the slight shear orientation of the rod-shaped α -helical tail of myosin at the lower shear rate [32]. Meanwhile, the irregular Brownian motion of the molecules causes the disordered distribution of MPs, which also contributes to the higher viscosity. The apparent viscosity of MP sols showed a sharp drop with an increase in the shear rate, which might be attributed to the fact that MPs flowed along the orientation of shear force, and the protein molecular chain was gradually expanded, stretched and oriented, resulting in the easy slip of arranged MP molecules [20,33]. It was noteworthy that the U_{MP} -KGM sample showed the lowest viscosity in the range of 0.1 to 100 s⁻¹, suggesting that this dual modification of low-salt MP in which KGM addition was carried out prior to the ultrasonic treatment might impair the myosin tail associations and head interactions, and provided greater steric hindrance to block the interaction between MPs. This result could be related to the decrease in size of the mixed protein suspension and the slight reduction of electrostatic repulsion between MPs (Fig. 1D). However, the U_{MP} -KGM sample existed the highest viscosity, indicating the enhanced association and hydrodynamic interactions among MPs [32]. This result was consistent with the thermal aggregation characteristics of low-salt proteins (Fig. 3G-L).

3.8.2. Thermal gelling ability

The temperature-dependent (20 °C \sim 80 °C) dynamic rheological characteristics of proteins indicate protein gelling capacity. As seen in Fig. 4B, the storage modulus (G') of MPs showed three distinct stages. Firstly, G' reached a maximum at ~ 55 °C, corresponding to myosin head cross-linking. Secondly, the drastic decrease in G' (55 °C \sim 60 °C), possibly due to light meromyosin dissociation and the consequent increase in filament fluidity, indicating that the previously formed network structure temporarily collapsed. Thirdly, a continuous increase in G' from 60 °C to 80 °C resulting from the tail-to-tail cross-linking of light meromyosin. Compared with pure MP, the peak temperature of U_{MP} sample shifted slightly towards the left, but a greater final G' was seen, suggesting that ultrasonic treatment could increase the sensibility of MPs to heating, which was also consistent with results of chicken myosin [8]. However, the peak temperature of dual-modified samples shifted towards the right, and the U_{MP} -KGM group had the highest G' value in the terminal of the sweep, indicating a stronger gel structure. Predictably, the increase in G' of different treated MPs could be attributed to the effects of hydrophobic interactions and disulfide bonds, indicating that KGM modification or ultrasonic treatment promoted the structural unfolding and crosslinking of MP molecules. The minimum G' of U_{MP} -KGM sample could be explained by the results in Figs. 1 and 4A, where this dual modification caused the formation of a uniform and soluble mixture, suggesting that the dual modification (U_{MP} -KGM) that KGM addition was carried out prior to the ultrasonic treatment slightly weakened the thermal aggregation of MPs.

The loss modulus (G'') characterizes the viscosity characteristics of the protein sol system. Higher G'' values were seen in all treated MPs excluding the U_{MP} -KGM sample in comparison with the control during the thermal gelation process, and the U_{MP} -KGM sample exhibited the maximum G'' (Fig. 4C). As shown in Fig. 4D, all MP samples had a $\tan\delta$ value that was lower than 1, indicating the notable elastic characteristics of MP sols during heating. The $\tan\delta$ level of all MP samples exhibited an obvious increase between 30 °C and 55 °C, demonstrating the formation of viscous MP sol caused by the degeneration of myosin tails [17]. Importantly, the groups of MP-KGM, U_{MP} , and U_{MP} -KGM demonstrated lower $\tan\delta$ values during the initial heating stage, indicating the presence of fine aggregation and cross-linking between protein molecules. Additionally, the U_{MP} -KGM gel exhibited maximum values of G' and G'' as well as lower initial $\tan\delta$, suggesting that the combination of KGM with pre-ultrasound contributed to the formation of viscoelastic composite gels.

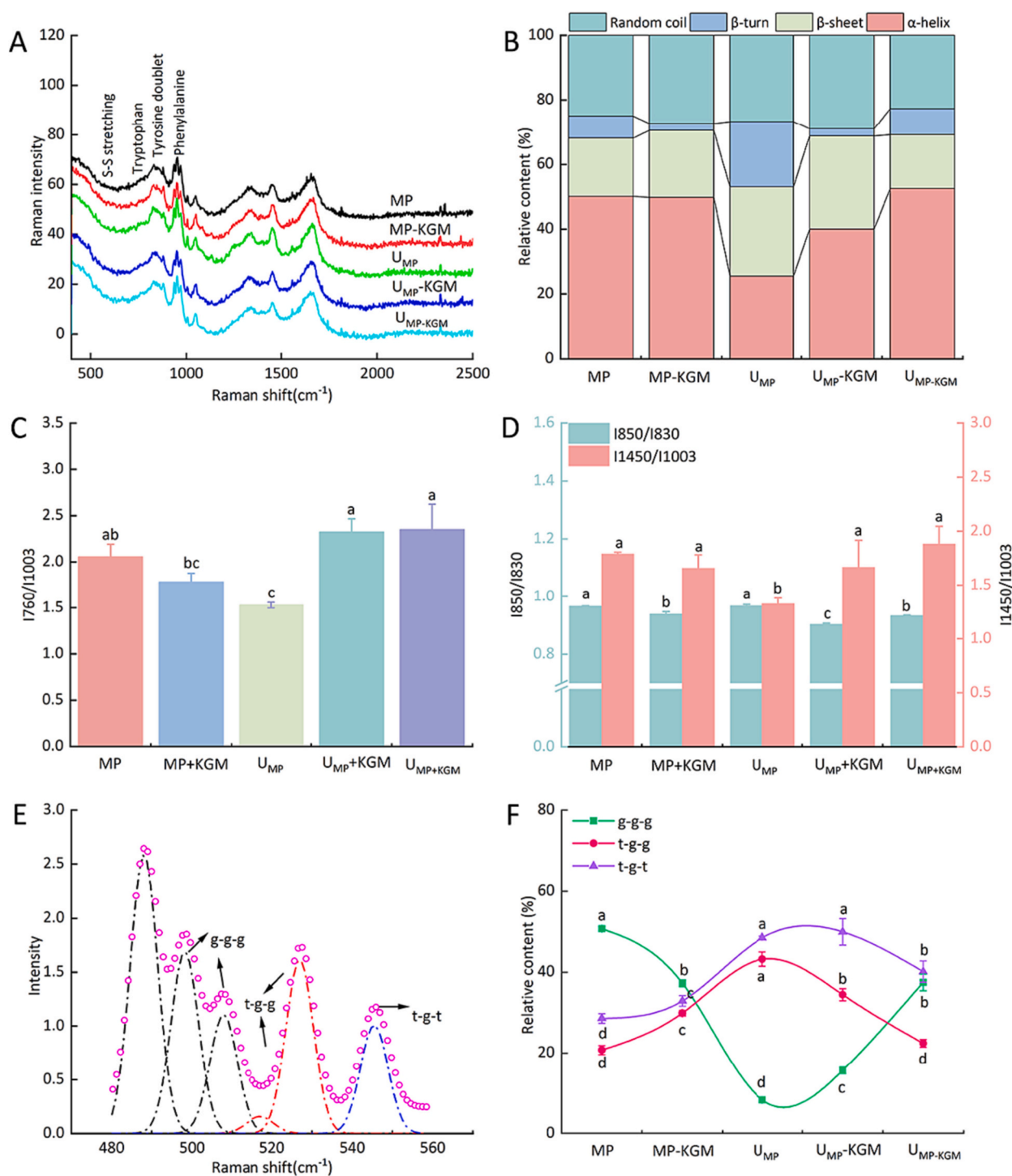


Fig. 5. The protein conformational analysis of MP gels. A: changes in the Raman spectra of MP gels. B: the percentage of secondary structure in MP gels. Normalized Raman spectral intensities of different treated MP gels (C: I760/1003, D: I850/830 and I1453/1003). The distribution of disulfide bond conformations (E) and the relative percentage of three S—S conformations (F). Error bars refer to the standard deviations. Different lowercase letters represent significant differences ($P < 0.05$).

3.9. Gelation properties

3.9.1. Water holding capacity and cooking loss

The water holding capacity of all treated protein gel samples showed an increasing tendency compared with the control (Fig. 4E), which might be due to the enhanced affinity of water-MPs and the crosslinking of exposed MP residues via hydrogen bonds and hydrophobic interactions. The maximum WHC (86.68 %) was obtained in the U_{MP}-KGM group, indicating that this modification in which ultrasound was carried

out before KGM addition induced a dense and well-structured three-dimensional gel network. This might be explained by the findings in Fig. 6, where U_{MP}-KGM modification induced a compact and homogeneous gel topology. In addition, Kim and his colleagues reported that the lower cooking loss might cause a higher WHC of the protein gel, which could induce soft textural properties of MP gels when this portion of water cannot be effectively retained in the gel matrix [34]. Similarly, the water-holding capacity of U_{MP}-KGM gel network was poor as compared with the U_{MP}-KGM sample, implying the relatively soft characteristics of

U_{MP}-KGM gel.

Cooking loss is intimately connected to the water holding potential of proteins throughout the heating process. The MP-KGM and U_{MP}-KGM modification significantly inhibited the moisture loss as compared to the pure MP gel (Fig. 4E). The reduction in cooking loss of MP-KGM gel indicated that the appearance of moisture channels was lessened during the thermally gelling process. In addition, the incorporation of KGM could enhance the water entrapment in the gel matrix owing to its abundant hydrophilic groups. The decrease in cooking loss of U_{MP}-KGM sample could be due to the smaller size of protein particles in sample suspension and the higher interaction between protein and water molecules during gelation. Therefore, water molecules are firmly trapped in the small pores of MP gel network, which was analogous to the results mentioned by Amiri and his colleagues [35].

3.9.2. Gel strength and texture characteristics

Gel strength is a noteworthy indicator to evaluate the properties of protein gel, which is closely associated with thermal protein aggregation and the ultimate meat product quality. The KGM modification and ultrasonic treatment significantly enhanced the gel strength of low-salt protein gels, with the strongest development occurred in the U_{MP}-KGM group (Fig. 4F). In addition, there were no discernible differences ($P > 0.05$) in the gel strength between U_{MP}-KGM sample and the control, implying that U_{MP}-KGM modification had no obvious effect on gel properties, probably due to that KGM was uniformly covered on the protein surface, which affected the thermal gelation process of MPs. Simultaneously, researchers reported that KGM might be entrapped as a filler ingredient and influenced the development of continuous gel, thus altering the aqueous phase distribution and improving the texture characteristics of MP gels [11]. Meanwhile, similar gel strength enhancement was also found in the PSE-like chicken breast treated with high-intensity ultrasound, which might be due to the higher pH value of MP after ultrasonic treatment [36].

The textural features relate to the composition and microstructure of the gel matrix, which are crucial in evaluating processed meat quality. Hardness represents the force applied to deform the sample. Chewiness is defined as the energy required to masticate sample to a state suitable for swallowing, which is a comprehensive expression of hardness, springiness, and cohesiveness. Compared with the control gel, the TPA parameters of modified protein gels were increased, particularly in the U_{MP}-KGM group (Fig. S2). It was possible that KGM exhibited excellent water absorption properties and acted as “fillers”, contributing positively to the effective occurrence of protein crosslinking and compact gel matrix. Furthermore, ultrasound could reduce protein size and induce the exposure of active groups, which increased MP-water and MP-MP interactions, resulting in the uniform and dense gel network accompanied by higher water-holding characteristics (Fig. 4E). Compared with U_{MP} gel, the textural properties of U_{MP}-KGM were further increased, which might be attributed to that the pre-ultrasonic treatment promoted the interaction between KGM and MPs (Fig. 1B), leading to the enhancement in gel properties. Additionally, the U_{MP}-KGM gel showed weaker textural characteristics as compared to other modified MP gels (MP-KGM, U_{MP}, U_{MP}-KGM). It might be attributed to the breakdown of polysaccharide molecule chain in MP-KGM suspension during ultrasound, which can be supported by the results of CLSM (Fig. 6), and the intrinsic mechanism was analyzed in detail below. Analogously, ultrasound-assisted Fenton method modified apricot polysaccharide had little effect on enhancing the properties of soy protein isolate gel as compared with the same concentration of apricot polysaccharide [37]. This result might be attributed to the lower branching degree and smaller molecular weight of the modified apricot polysaccharide, leading to the relatively weak conformational change of the protein.

3.9.3. Thermodynamic properties of MP gels

The thermostability of protein gel is often used to appraise the interaction between sample components, reflecting the thermodynamic

transformation and denaturation of proteins. The control gel revealed an endothermal peak at 40.2 °C, as shown in Fig. S2G, which was ascribed to the myosin denaturation. The endothermic transition peak increased after KGM addition, suggesting that KGM enhanced the thermal stability of MP gel by altering protein conformation, which was also supported by the increased water-holding capacity of protein gel in Fig. 4E. This phenomenon was similar with Ran and his colleagues, who mentioned that KGM delayed the denaturation of soy protein, promoted protein aggregation, and enhanced the gelling temperature [38]. Additionally, compared to the control protein gel, the endothermic peaks of ultrasound treated protein gels (U_{MP}, U_{MP}-KGM, U_{MP}-KGM) transferred to elevated temperatures of 44.76 °C, 45.16 °C, and 43.79 °C, respectively. Similarly, the thermal degeneration of golden threadfin bream myofibrillar protein was retarded after ultrasonic treatment [39]. The reason for this phenomenon may be due to the unfolding of myosin heads caused by ultrasound, which induced a relatively stable protein structure with a higher proportion of β -sheet, leading to the formation of a thermally stable gel matrix. Especially, the improvement of thermal stability in modified protein gels (MP-KGM, U_{MP}, U_{MP}-KGM, U_{MP}-KGM) was similar with the trend of protein thermal aggregation behavior (Fig. 3G-L).

3.9.4. Secondary structure in protein gels

The characteristics of protein gel are intimately connected to protein structure changes, which can be well reflected by Raman spectroscopy. The peaks corresponding to protein secondary structure were mainly specified as α -helix (1650–1658 cm⁻¹), β -sheet (1665–1680 cm⁻¹), β -turn (1680–1690 cm⁻¹), and random coil (1660–1665 cm⁻¹) from the amide I band (1600–1700 cm⁻¹). Based on this, the percentage of secondary structure was estimated, and the results were displayed in Fig. 5B. Compared with the pure protein gel, the quantitative analysis demonstrated a decrease in α -helix percentage accompanied by an increased β -sheet proportion of the blend gel (MP-KGM), indicating that KGM addition promoted the unfolding of MP during thermal gelation process. Similar results were reported when KGM was added to pork MP [28]. The ultrasound-treated groups (U_{MP}, U_{MP}-KGM) also showed the transition of α -helix to a looser β -sheet, suggesting that MP might be stretched and interacted with other molecules through hydrophobic interaction and hydrogen bond due to the cavitation effect, which was similar to the results of Kang and his colleagues [40]. The U_{MP}-KGM group exhibited the highest β -sheet proportion, indicating an increase in ordered structure proportion. Similar results were mentioned by Shi and his colleagues, who discovered that ultrasound combined with potassium alginate marination also manifested more β -sheets and fewer α -helices [41]. Therefore, secondary structure changes of the U_{MP}-KGM gel sample corresponded to the improved three-dimensional structure, which was corresponded to our WHC results (Fig. 4E).

3.9.5. Local environments in MP gels

The characteristic bands of tryptophan (around 760 cm⁻¹), tyrosine doublet (nearby 830 cm⁻¹ and 850 cm⁻¹), and aliphatic residues such as -CH₂-, -CH₃, and = C-H bending (around 1450 cm⁻¹) in Raman spectroscopy could be analyzed to monitor the microenvironmental polarity around amino acids and the level of hydrogen bond involvement. The normalized intensities of above residues (I760/1003, I850/830, I1450/1003) in low-salt MP gels were shown in Fig. 5C-D. The Raman band approximately at 760 cm⁻¹ was attributed to the stretching and vibration of indole ring in tryptophan residues, and the I760/1003 intensity could reflect the hydrophobicity of tryptophan residues and the hydrophobic interaction in MP gel. When compared with the control, the I760/1003 intensity was significantly decreased to 1.78 ± 0.13 and 1.52 ± 0.04 in MP-KGM and U_{MP} groups (see Fig. 5C), respectively, suggesting that the initially buried tryptophan group in MPs were exposed to the polar microenvironment and the hydrophobic interaction between tryptophan residues was increased [42]. The strength of I760/1003 for dual-modified protein gels (U_{MP}-KGM, U_{MP}-KGM) was enhanced

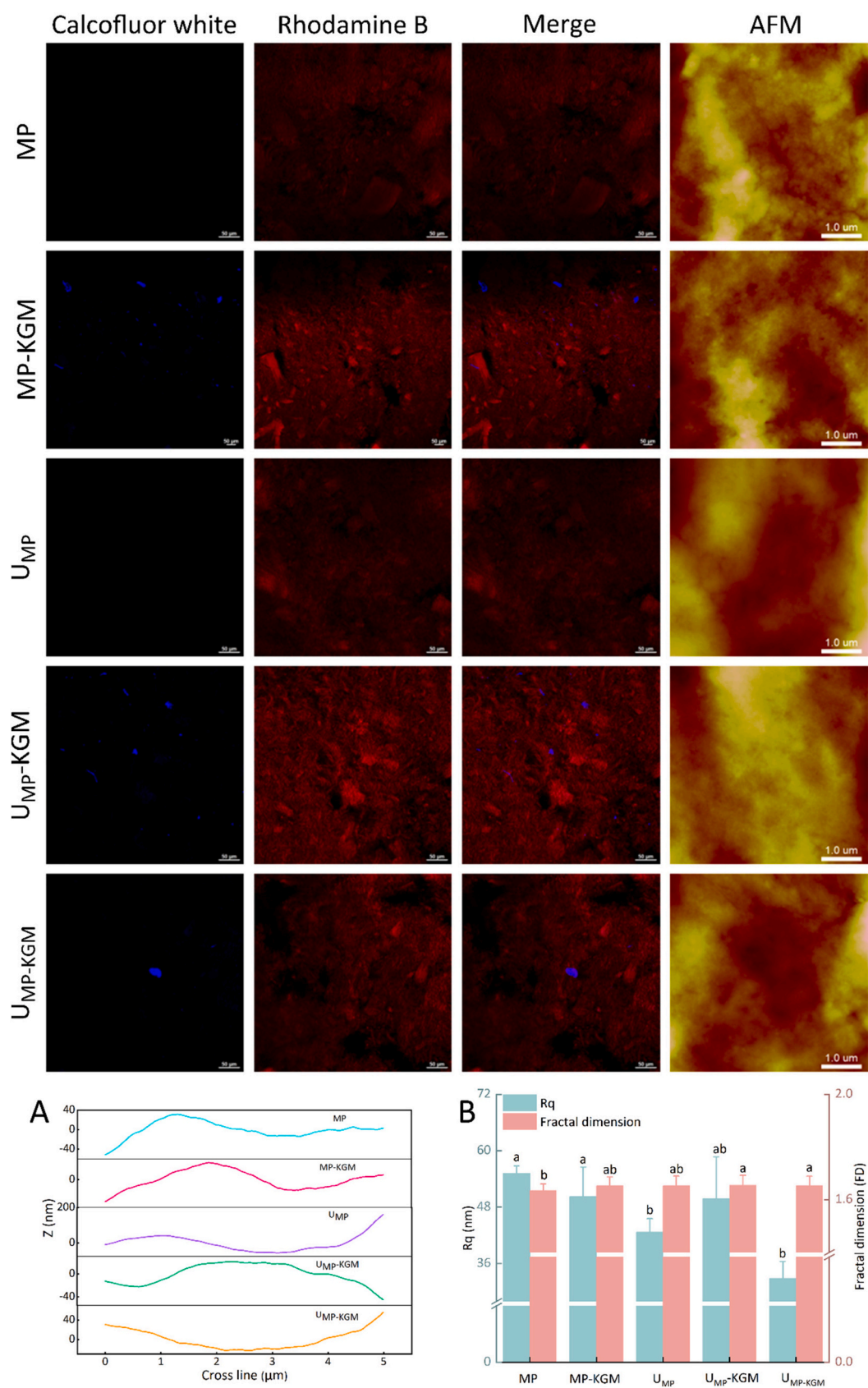


Fig. 6. The CLSM images and surface topological morphology of MP gels (MP, MP-KGM, U_{MP}, U_{MP}-KGM, U_{MP}-KGM), the step analysis curves (A) corresponding to each AFM height image (Last column), and the fractal dimension and Rq of MP gels according to corresponding AFM images (B). KGM was labelled with Calcofluor white (First column), protein was dyed with Rhodamine B (Second column), and the overlap images for protein and KGM (Third column). Different lowercase letters represent significant differences ($P < 0.05$).

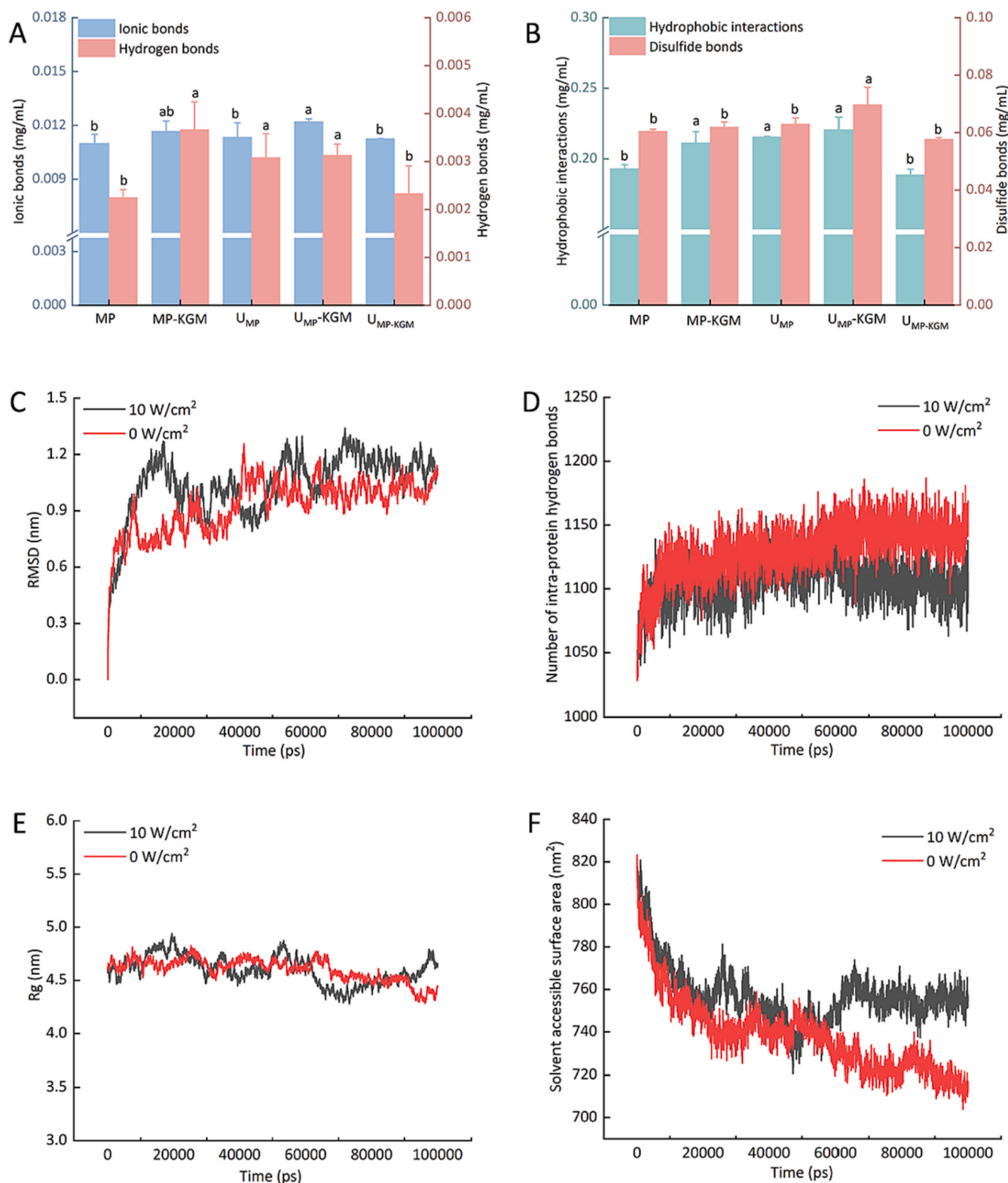


Fig. 7. Intermolecular forces (A: ionic bonds and hydrogen bonds; B: hydrophobic interactions and disulfide bonds) in MP gels. The molecular dynamics simulation of myosin before and after ultrasound treatment (C–F). The RMSD (C), intramolecular hydrogen bond (D), Rg (E), and solvent accessible surface area (SASA, F) of the myosin at 0 and 10 W/cm² over simulation time.

as compared to the control group ($P > 0.05$), suggesting that more hydrophobic tryptophan groups were trapped in the hydrophobic micro-environment. The increase in I760/1003 strength of dual-modified protein gels might result from the attachment of KGM molecules on the protein surface, which corresponded to the results of tryptophan

fluorescence (Fig. 1A).

The ratio of tyrosine doublet bands (1850/1830) was used to monitor the exposure (ratio ranging from 0.9 to 1.45) or burial (from 0.7 to 1.0) of tyrosine residues, reflecting the changes of hydrogen bonds formed by tyrosine -OH groups with water molecules or with other residues in MP

gels. It was shown that the I850/830 intensity varied from 0.94 to 0.97 in all MP gel samples (Fig. 5D), indicating that the -OH groups in protein gel generated hydrogen bonds with other residues. In comparison with the control group, the intensity of I850/830 in composite protein gels (MP-KGM, U_{MP}-KGM, U_{MP}-KGM) decreased, possibly due to the adhesion of polysaccharide to MPs, thus resulting in the burying of tyrosine groups and the strengthened hydrogen bonds formed by -OH groups with other groups. However, no appreciable variations were found in the I850/1830 intensity between control and U_{MP} group ($P > 0.05$).

The decreased intensity of the I1450/1003 ratio could suggest the formation of hydrophobic associations around aliphatic residues in protein gel. As seen in Fig. 5D, the intensity of I1450/1003 in the group of MP-KGM, U_{MP}, and U_{MP}-KGM decreased and the U_{MP} group had the minimum I1450/1003 ratio, which implied the enhancement of hydrophobic interactions between MP molecules, thus resulting in the improved network structure (Fig. 4B) and water holding capacity (Fig. 4E) of protein gels. A possible reason is that the internal cross-linking of aliphatic residues was increased via hydrogen bond interaction. This result was consistent with those reported by Zhang and his companions, who reported that KGM addition (1 %) facilitated protein unfolding and enhanced hydrophobic interactions during thermal processing, thus inducing the development of a compact and homogeneous gel structure [11]. However, compared with the control, the intensity at 1450 cm^{-1} in U_{MP}-KGM sample was increased by 4.9 % ($P > 0.05$), implying that the hydrophobic associations of aliphatic groups were slightly weakened in the dual-modified protein gel when KGM was added before ultrasonic treatment.

3.9.6. Disulfide bridges (S—S) conformation in MP gels

The formation and conversion of both intramolecular and intermolecular S—S bonds are crucial to the conformation and activity of MPs due to that they are important targets for the crosslinking between MPs that occurs during the thermal gelation process. Based on the varying conformations of S—S bridges, the $490\text{--}560\text{ cm}^{-1}$ region has been referred to gauche-gauche-gauche conformation (around 490 cm^{-1} , g-g-g), trans-gauche-gauche (around 520 cm^{-1} , t-g-g) and trans-gauche-trans (around 550 cm^{-1} , t-g-t) separately (Li et al., 2019). Deconvoluted spectra of the S—S region (around $490\text{--}560\text{ cm}^{-1}$) and proportion of three S—S configurations for protein gels were presented in Fig. 5E and Fig. 5F, respectively. The control protein gel dominated g-g-g conformation with lower potential energy, implying a stable protein conformation. The g-g-g and t-g-g configurations represent intramolecular disulfide bridges, while the t-g-t is an intermolecular disulfide bond, and changes in the disulfide bond conformation may be connected to the energy transition and protein structure. Compared with the control sample, the relative percentage of g-g-g in all treated MP gels was reduced with a concurrent increase in t-g-g and t-g-t conformations except the U_{MP}-KGM gel sample, implying changes in MP conformation. Importantly, the U_{MP}-KGM sample existed the highest percentage content in t-g-t, indicating the ordered thermally-induced gelling behavior of MPs, which corresponded to the results as shown in Fig. 4B. In addition, the previous study reported suggested that proteins with larger percentage of α -helices primarily display g-g-g configuration. Consequently, the remarkable transformation from g-g-g to t-g-t configuration in U_{MP}-KGM group corresponding to the maximum proportion of β -sheet transformed by α -helix (Fig. 5B), suggesting that the gelling potential of proteins was closely connected to t-g-g and t-g-t conformations.

3.9.7. Topology of MP gels

Investigating the characteristics of thermally induced protein gel requires consideration of topology [19]. Rq is a measure of average roughness that was derived from the heights of each spot throughout the whole image region. As shown in Fig. 6, the roughness (Rq) and fractal dimension (FD) were obtained by analyzing the AFM height images of low-salt MP gels. The light and dark regions in height images indicate convex and concave surfaces on the gel surface, respectively. The control

protein gel showed a fibrous surface morphology, suggesting the disordered aggregation of proteins during the heating process and the formation of large irregular MP aggregates. When compared to the control protein gel, modified composite gel samples (MP-KGM, U_{MP}, U_{MP}-KGM, U_{MP}-KGM) had a smoother surface with lower roughness (Rq) values. The Rq value of the control was $55.20 \pm 1.56\text{ nm}$ (Fig. 6B). Meanwhile, the Rq value of protein gels in MP-KGM, U_{MP}, U_{MP}-KGM, and U_{MP}-KGM groups decreased to $50.25 \pm 6.29\text{ nm}$, $28.30 \pm 6.93\text{ nm}$, $49.85 \pm 8.84\text{ nm}$, and $32.85 \pm 3.61\text{ nm}$ individually. Fractal dimension characterizes gel surface complexity, which can be estimated based on the AFM grayscale image of protein gel, was utilized to describe the surface complexity [19]. The fractal dimension of protein gels increased in MP-KGM, U_{MP}, U_{MP}-KGM, and U_{MP}-KGM groups, which indicated that KGM addition, ultrasound treatment and dual modification increased gel surface complexity. The increase in fractal dimension might be due to that above modification promoted MP unfolding and enhanced interactions between hydrophobic groups during gelation, resulting in a compact and homogeneous gel network. Similar results were reported in silver carp surimi pre-treated by ultrasound [43]. In addition, KGM could further reduce water channels in the composite gel matrix and promote the interaction between hydrophobic groups, which facilitated the formation of a more continuous gel matrix, and was congruent with the findings of WHC (Fig. 4E).

3.9.8. Microstructural observation

The microstructural visualization of protein gel sample was depicted in Fig. 6. Myofibrillar protein labelled with Rhodamine B was seen as red, while the blue represented KGM molecules dyed with Calcofluor white. The control gel exhibited a continuous morphology with a uniform red fluorescence. Compared with the control, proteins in groups of MP-KGM, U_{MP}, U_{MP}-KGM, and U_{MP}-KGM became more aggregated, implying the enhanced protein intermolecular interactions (Fig. 7A-B). Obviously, KGM was distributed in the complex protein system in the MP-KGM and U_{MP}-KGM group, where KGM was embedded in the protein network in the U_{MP}-KGM group, suggesting enhanced protein-polysaccharide interactions and denser gel structure (Fig. 4F). The enhanced crosslinking of proteins and abundant hydrophilic groups of KGM were the major causes of a dense and well-structured three-dimensional network in U_{MP}-KGM gel. Besides, the most important findings were the decreased fluorescence intensity of KGM in U_{MP}-KGM group, suggesting the disruption of KGM structure and weakened biopolymer interactions. These results concurred with those reported by Xu and his associates [37], who discovered that modified apricot polysaccharide (ultrasound-assisted Fenton method) possessed little effect on improving the properties of soy protein isolate gel due to the reduced branching degree of apricot polysaccharide.

3.9.9. Intermolecular forces in protein gels

The properties of gel matrix depend on the intermolecular force equilibrium between proteins and other proteins and with water molecules. Results showed that the proportion of intermolecular forces in different low-salt MP gels was significantly different (Fig. 7A-B). Obviously, the hydrophobic association was the dominant force in the MP gel, followed by disulfide bond, ionic bond, and a lesser content of hydrogen bond. The proportion of hydrogen and ionic bonds was relatively low, which may be due to the destruction caused by thermal gelation. Compared to the control gel, the content of aforementioned four forces in modified MP gels increased significantly after KGM modification or ultrasound treatment (MP-KGM, U_{MP}, U_{MP}-KGM), demonstrating the unfolding of MPs (Fig. 5B) and the improved stability of protein gel, which was corresponded to the findings of gel strength (Fig. 5F). Previous study reported that hydroxyl groups on KGM molecules might form stronger hydrogen bonds with protein subunits, which delayed protein denaturation and facilitated the adequate expose of functional groups, resulting in enhanced intermolecular forces of hydrogen bonds, hydrophobic interactions, and disulfide bonds. In

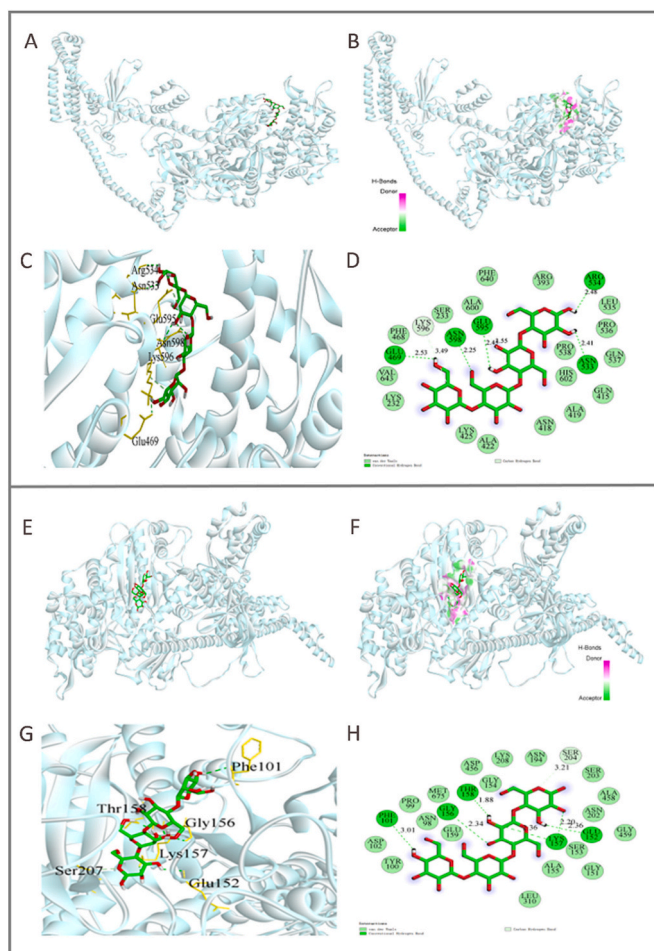


Fig. 8. The optimum docking model between KGM and myosin molecules produced by molecular dynamics simulation under different ultrasound intensities of 0 (A) and 10 W/cm² (E). Green represents KGM, while grayish blue represents myosin at 0 and 10 W/cm², respectively. The H-Bonds (B, F), 3D diagram (C, G), and 2D schematic diagram (D, H) of the interaction between KGM and myosin (B-D: 0 W/cm², F-H: 10 W/cm²). (For interpretation of the references to colour in this figure legend, the reader is referred to the web version of this article.)

addition, the improved four intermolecular forces in ultrasound treated gel sample (U_{MP}) may result from the effective exposure of sulfhydryl groups, charged amino acid groups, and hydrophobic groups. Generally, hydrogen bond contributes to stabilize water molecules and enhance the water-holding capacity of gel samples. The increased hydrophobic interaction and disulfide bond reflect the exposure of hydrophobic sidechains and sulfhydryl residues, respectively, in relation to the better gelling properties. Importantly, the stronger intermolecular forces in U_{MP} -KGM gel were in accordance with the enhanced gel properties (Fig. 4), supporting the effect of KGM combined with pre-ultrasound in modulating the protein conformation of MP gel at the low-salt level. Nevertheless, KGM combined with subsequent ultrasound treatment (U_{MP} -KGM) seemed to be detrimental to the stability of gel matrix, as evidenced by the weak hydrophobic interaction and disulfide bond, which was consistent with the local environments in MP gels.

3.10. Molecular dynamics simulations

The deviation of root-mean-square-deviation (RMSD) reflects the structural deviation of the main atom from the starting position to other position under different conditions during the simulation process, which is used to evaluate the structural stability of proteins. The higher RMSD

value implied an unstable protein structure with larger changes in molecular conformation [44]. Results showed that the RMSD value fluctuated significantly in the range of 0–20,000 ps (Fig. 7C). Besides, the RMSD value of 10 W/cm² group was greater than that of 0 W/cm² group at the equilibrium point (100,000 ns) in the simulation process, indicating the conformational changes and decreased stability of protein after ultrasonic treatment, which was consistent with the reduced proportion of α -helix (Fig. 1C-D). In addition, hydrogen bond is crucial for maintaining the stability of protein secondary structure. Compared with pure protein, the number of intramolecular hydrogen bonds in the 10 W/cm² group possessed a downward trend, which was approximately 1113 at the equilibrium (Fig. 7D). The decrease in intramolecular hydrogen bonds may be owing to the destruction of protein caused by ultrasonic treatment. The Rg and solvent accessible surface area (SASA) indicate the tightness degree of proteins. The utmost distance between atom and the geometric center of protein is usually expressed as the Rg value. During the simulation process, the Rg value in 0 W/cm² group fluctuated slightly, indicating that the protein structure was relatively stable (Fig. 7E). When equilibrium was reached after ultrasonic treatment (10 W/cm²), the Rg value increased markedly, implying that ultrasound treatment weakened the internal interaction and reduced the structural stability of proteins. Importantly, the Rg level was consistent with the trend of intramolecular bond number, which can be validated by the results of protein secondary and tertiary structure (Fig. 1). As an important functional property of protein, the surface property affects the interaction between protein and other substances. A higher solvent accessible surface area (SASA) value was observed in the 10 W/cm² group as compared with 0 W/cm² group (Fig. 7F), indicating the unfolding of protein structure after ultrasound treatment. Analogously, the exposure of protein residues altered the protein binding site and increased the surface property of protein, thereby enhancing protein activity [45].

3.11. Molecular docking of KGM and myofibrillar protein

The binding pattern and affinity between molecules (receptor and ligand) can be predicted by Molecular docking. It is generally believed that the higher absolute value of binding energy, the higher the binding affinity. As exhibited in Fig. 8, KGM bound well to the myosin with high coordination and the binding energy of both 0 W/cm² and 10 W/cm² groups was -8.5 kcal/mol. The binding affinities of both groups were less than -5 kcal/mol, indicating that the ligand and the selected protein receptor had a good binding effect. The surface and bonding interface of KGM and myosin for the active site were shown in Fig. 8A-H. At 0 W/cm², KGM could form strong hydrogen bonding interactions with Arg-534, Asn-533, Glu-595, Asn-598, Lys-596, and Glu-469 in the active site of myosin (Fig. 8D). Furthermore, KGM could form strong hydrogen bonding interactions with Phe-101, Thr-158, Gly-156, Lys-157, Ser-207, and Glu-152 in the active site of myosin treated by ultrasound (Fig. 8H). The formation of hydrogen bonds was crucial for the anchoring of small molecules in the protein pocket [44]. It can be clearly observed that KGM and myosin formed multiple binding bonds, and the number of hydrogen bonds between two groups of proteins and KGM was consistent. Importantly, the average bond length of hydrogen bonds in the 10 W/cm² group was shorter than that in the 0 W/cm² group, indicating that ultrasound treated protein and KGM were bound tightly, which can also be supported by the results of CLSM. Consequently, the interaction sites between protein and KGM were altered by ultrasound pretreatment, and these interactions might contribute to enhance the stability of complex.

4. Conclusions

In this research, the conformational characteristics of protein were modulated by single and double sequential modifications using KGM and ultrasound to prepare the low-salt MP gel with excellent gelling

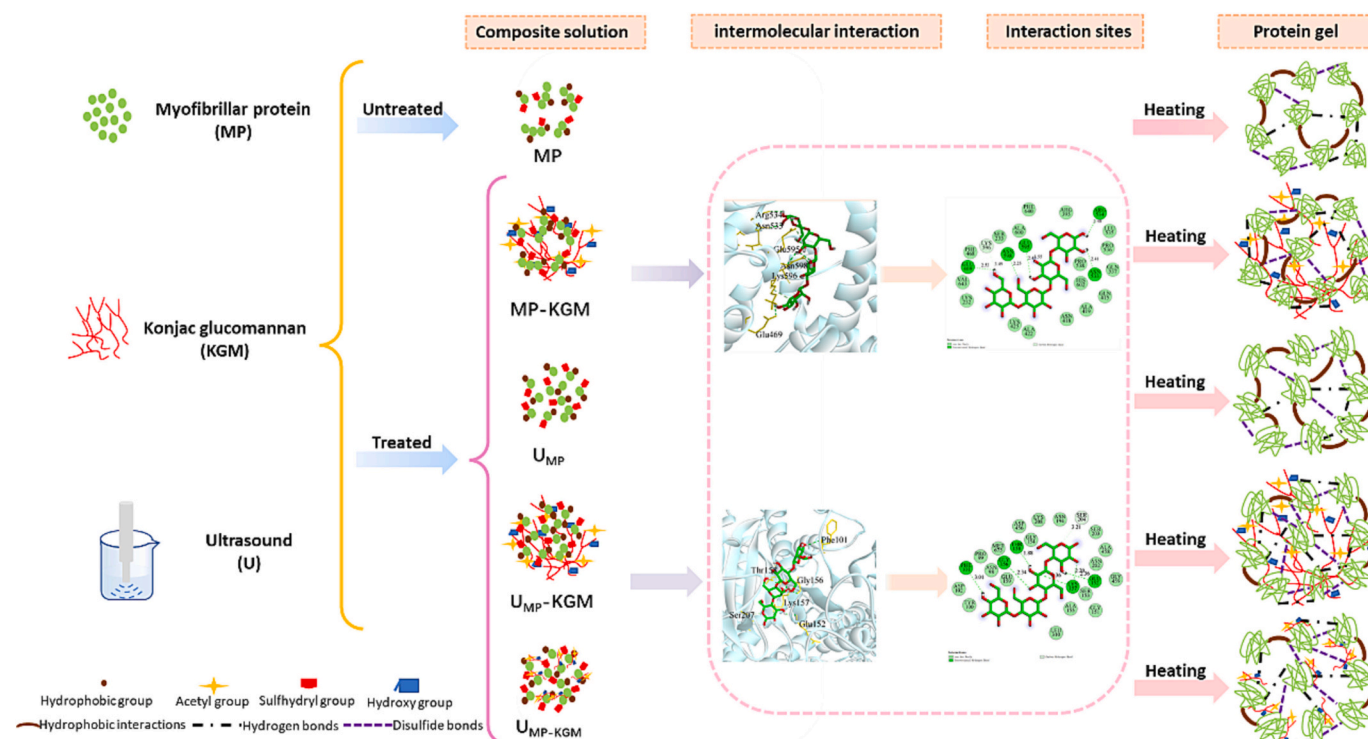


Fig. 9. Proposed schematic illustration depicting the influence of single and double sequential modification by utilizing KGM and ultrasound on the formation of protein gels under the low-salt condition.

properties. Specifically, single KGM modification or ultrasound treatment caused the exposure of more tryptophan groups and hydrophobic residues. Moreover, ultrasound pre-treatment combined with KGM modification increased the thermal aggregation of MPs, improved the hydrophobic interaction of aliphatic residues, and strengthened the formation of intramolecular hydrogen bonds, which facilitated the rheological and gelling characteristics of low-salt MPs. Importantly, further molecular dynamic simulation and molecular docking analysis proved that ultrasound pre-treatment enhanced the association between KGM and low-salt MP, as depicted in Fig. 9. However, the uniformity of the MP-KGM mixture induced by ultrasound treatment relatively weakened protein unfolding and thus had limited effect on improving the characteristics of low-salt MP gel, as evidenced by the disruption of KGM molecules and the weakening of intermolecular interactions observed by confocal laser microscopy. Consequently, the combination of ultrasound pre-treatment and subsequent KGM modification is recommended to enhance the quality of processed low-salt meat products. This study can help guide the application of KGM and ultrasound treatment in the manufacturing of low-salt meat products to ameliorate textural defects caused by low-sodium salt.

CRediT authorship contribution statement

Yongfang Gao: Data curation, Methodology, Writing-original draft. Yunpeng Hu: Methodology. Jiakuan Wang: Sample preparation. Hafiz Nabeel Ahmad: Editing-review. Jie Zhu: Project administration, Resources, Review, Editing, Supervision.

Declaration of competing interest

The authors declare no conflict of interest.

Data availability

The authors do not have permission to share data.

Acknowledgements

This project was supported by the Central Government Guided Local Science and Technology Development Fund of Shaanxi Province (2022Yangling-001, JZ), and the Research Program of Science and Technology of Haiyuan County, Ningxia Hui Autonomous Region (2022HYKJJH005, JZ). Special thanks to Prof. Zan at NBCIC of NWAUFU for his supports and suggestions.

Appendix A. Supplementary data

Supplementary data to this article can be found online at <https://doi.org/10.1016/j.ijbiomac.2023.126195>.

References

- [1] Y. Cao, Z. Li, B. Li, X. Fan, M. Liu, J. Zhao, Mitigation of oxidation-induced loss of myofibrillar protein gelling potential by the combination of pyrophosphate and l-lysine, *LWT* 157 (2022), 113068, <https://doi.org/10.1016/j.lwt.2022.113068>.
- [2] Y. Sun, L. Ma, Y. Fu, H. Dai, Y. Zhang, The improvement of gel and physicochemical properties of porcine myosin under low salt concentrations by pulsed ultrasound treatment and its mechanism, *Food Res. Int.* 141 (2021), 110056, <https://doi.org/10.1016/j.foodres.2020.110056>.
- [3] F.J. He, G.A. Macgregor, Role of salt intake in prevention of cardiovascular disease: controversies and challenges, *Nat. Rev. Cardiol.* 15 (2018) 371–377, <https://doi.org/10.1038/s41569-018-0004-1>.
- [4] N. Zhao, H. Zou, S. Sun, C. Yu, The interaction between sodium alginate and myofibrillar proteins: the rheological and emulsifying properties of their mixture, *Int. J. Biol. Macromol.* 161 (2020) 1545–1551, <https://doi.org/10.1016/j.ijbiomac.2020.08.025>.
- [5] J.A. Gómez-Salazar, A. Galván-Navarro, J.M. Lorenzo, M.E. Sosa-Morales, Ultrasound effect on salt reduction in meat products: a review, *Current Opinion in Food Science* 38 (2021) 71–78, <https://doi.org/10.1016/j.cofs.2020.10.030>.
- [6] L. Mirmoghtadaie, S. Shojae Aliabadi, S.M. Hosseini, Recent approaches in physical modification of protein functionality, *Food Chem.* 199 (2016) 619–627, <https://doi.org/10.1016/j.foodchem.2015.12.067>.
- [7] Z. Zhang, J.M. Regenstein, P. Zhou, Y. Yang, Effects of high intensity ultrasound modification on physicochemical property and water in myofibrillar protein gel, *Ultrason. Sonochem.* 34 (2017) 960–967, <https://doi.org/10.1016/j.ultsonch.2016.08.008>.

- [8] J.Y. Wang, Y.I. Yang, X.Z. Tang, W.X. Ni, L. Zhou, Effects of pulsed ultrasound on rheological and structural properties of chicken myofibrillar protein, *Ultrason. Sonochem.* 38 (2017) 225–233, <https://doi.org/10.1016/j.ultsonch.2017.03.018>.
- [9] Y. Xiong, Q. Li, S. Miao, Y. Zhang, B. Zheng, L. Zhang, Effect of ultrasound on physicochemical properties of emulsion stabilized by fish myofibrillar protein and xanthan gum, *Innovative Food Sci. Emerg. Technol.* 54 (2019) 225–234, <https://doi.org/10.1016/j.ifset.2019.04.013>.
- [10] M.A. Iglesias-Otero, J. Borderías, C.A. Tovar, Use of Konjac glucomannan as additive to reinforce the gels from low-quality squid surimi, *J. Food Eng.* 101 (2010) 281–288, <https://doi.org/10.1016/j.jfoodeng.2010.07.009>.
- [11] X. Zhuang, X. Jiang, H. Zhou, Y. Chen, Y. Zhao, H. Yang, G. Zhou, Insight into the mechanism of physicochemical influence by three polysaccharides on myofibrillar protein gelation, *Carbohydr. Polym.* 229 (2020), 115449, <https://doi.org/10.1016/j.carbpol.2019.115449>.
- [12] Y. Gao, C. Luo, J. Zhang, H. Wei, L. Zan, J. Zhu, Konjac glucomannan improves the gel properties of low salt myofibrillar protein through modifying protein conformation, *Food Chem.* 393 (2022), 133400, <https://doi.org/10.1016/j.foodchem.2022.133400>.
- [13] S.M.H. Hosseini, Z. Emam-Djomeh, S.H. Razavi, A.A. Moosavi-Movahedi, A. A. Saboury, M.S. Atri, P. Van der Meer, β -Lactoglobulin–sodium alginate interaction as affected by polysaccharide depolymerization using high intensity ultrasound, *Food Hydrocoll.* 32 (2013) 235–244, <https://doi.org/10.1016/j.foodhyd.2013.01.002>.
- [14] J. Chen, X. Chen, G. Zhou, X. Xu, Ultrasound: a reliable method for regulating food component interactions in protein-based food matrices, *Trends Food Sci. Technol.* 128 (2022) 316–330, <https://doi.org/10.1016/j.tifs.2022.08.014>.
- [15] K. Li, L. Fu, Y.Y. Zhao, S.W. Xue, P. Wang, X.L. Xu, Y.H. Bai, Use of high-intensity ultrasound to improve emulsifying properties of chicken myofibrillar protein and enhance the rheological properties and stability of the emulsion, *Food Hydrocoll.* 98 (2020), 105275, <https://doi.org/10.1016/j.foodhyd.2019.105275>.
- [16] Y. Jiang, D. Li, J. Tu, Y. Zhong, D. Zhang, Z. Wang, X. Tao, Mechanisms of change in gel water-holding capacity of myofibrillar proteins affected by lipid oxidation: the role of protein unfolding and cross-linking, *Food Chem.* 344 (2021), 128587, <https://doi.org/10.1016/j.foodchem.2020.128587>.
- [17] H. Zhang, X. Li, S. Sun, Y. Wang, Z. Li, H. Kang, X. Peng, Effects of carboxymethyl chitosan on the oxidation stability and gel properties of myofibrillar protein from frozen pork patties, *Int. J. Biol. Macromol.* 234 (2023), 123710, <https://doi.org/10.1016/j.ijbiomac.2023.123710>.
- [18] Y. Zhong, P. Han, S. Sun, N. An, X. Ren, S. Lu, Q. Wang, J. Dong, Effects of apple polyphenols and hydroxypropyl- β -cyclodextrin inclusion complexes on the oxidation of myofibrillar proteins and microstructures in lamb during frozen storage, *Food Chem.* 375 (2022), 131874, <https://doi.org/10.1016/j.foodchem.2021.131874>.
- [19] Y. Hu, L. Zhang, Y. Yi, I. Solangi, L. Zan, J. Zhu, Effects of sodium hexametaphosphate, sodium tripolyphosphate and sodium pyrophosphate on the ultrastructure of beef myofibrillar proteins investigated with atomic force microscopy, *Food Chem.* 338 (2021), 128146, <https://doi.org/10.1016/j.foodchem.2020.128146>.
- [20] J. Chen, X. Zhang, S. Xue, X. Xu, Effects of ultrasound frequency mode on myofibrillar protein structure and emulsifying properties, *Int. J. Biol. Macromol.* 163 (2020) 1768–1779, <https://doi.org/10.1016/j.ijbiomac.2020.09.114>.
- [21] L. Jiang, Y. Ren, Y. Xiao, S. Liu, J. Zhang, Q. Yu, Y. Chen, J. Xie, Effects of Mesona chinensis polysaccharide on the thermostability, gelling properties, and molecular forces of whey protein isolate gels, *Carbohydr. Polym.* 242 (2020), 116424, <https://doi.org/10.1016/j.carbpol.2020.116424>.
- [22] N. Jia, F. Zhang, Q. Liu, L. Wang, S. Lin, D. Liu, The beneficial effects of rutin on myofibrillar protein gel properties and related changes in protein conformation, *Food Chem.* 301 (2019), 125206, <https://doi.org/10.1016/j.foodchem.2019.125206>.
- [23] Y. Zou, P. Xu, H. Wu, M. Zhang, Z. Sun, C. Sun, D. Wang, J. Cao, W. Xu, Effects of different ultrasound power on physicochemical property and functional performance of chicken actomyosin, *Int. J. Biol. Macromol.* 113 (2018) 640–647, <https://doi.org/10.1016/j.ijbiomac.2018.02.039>.
- [24] J. Chen, X. Zeng, X. Sun, G. Zhou, X. Xu, A comparison of the impacts of different polysaccharides on the sono-physico-chemical consequences of ultrasonic-assisted modifications, *Ultrason. Sonochem.* 96 (2023), 106427, <https://doi.org/10.1016/j.ultsonch.2023.106427>.
- [25] Y. Zou, F. Lu, B. Yang, J. Ma, J. Yang, C. Li, X. Wang, D. Wang, W. Xu, Effect of ultrasound assisted konjac glucomannan treatment on properties of chicken plasma protein gelation, *Ultrason. Sonochem.* 80 (2021), 105821, <https://doi.org/10.1016/j.ultsonch.2021.105821>.
- [26] S. Jiang, M. Zhang, H. Liu, Q. Li, D. Xue, Y. Nian, D. Zhao, K. Shan, C. Dai, C. Li, Ultrasound treatment can increase digestibility of myofibrillar protein of pork with modified atmosphere packaging, *Food Chem.* 377 (2022), 131811, <https://doi.org/10.1016/j.foodchem.2021.131811>.
- [27] S. Fan, J. Guo, X. Wang, X. Liu, Z. Chen, P. Zhou, Effects of lipoxigenase/linoleic acid on the structural characteristics and aggregation behavior of pork myofibrillar protein under low salt concentration, *LWT* 161 (2022), 113359, <https://doi.org/10.1016/j.lwt.2022.113359>.
- [28] X. Zhuang, X. Jiang, H. Zhou, M. Han, Y. Liu, Y. Bai, X.-L. Xu, G.H. Zhou, The effect of insoluble dietary fiber on myofibrillar protein emulsion gels: oil particle size and protein network microstructure, *LWT* 101 (2019) 534–542, <https://doi.org/10.1016/j.lwt.2018.11.065>.
- [29] W. Xia, L. Ma, X. Chen, X. Li, Y. Zhang, Physicochemical and structural properties of composite gels prepared with myofibrillar protein and lecithin at various ionic strengths, *Food Hydrocoll.* 82 (2018), <https://doi.org/10.1016/j.foodhyd.2018.03.044>. S0268005X18300195.
- [30] J. Zhang, J. Meng, X. Yun, T. Dong, Effect of Artemisia sphaerocephala Krasch gum on the gel properties of myofibrillar protein and its application in cooked sheep sausage, *Food Hydrocoll.* 142 (2023), 108752, <https://doi.org/10.1016/j.foodhyd.2023.108752>.
- [31] Z. Han, X. Li, Y. Liu, X. Yue, Z. Wu, J.-H. Shao, The evolution of pork myosin aggregates and the relationship between aggregation modes and microstructures of O/W emulsions, *Food Hydrocoll.* 119 (2021), 106825, <https://doi.org/10.1016/j.foodhyd.2021.106825>.
- [32] X. Chen, X. Xu, D. Liu, G. Zhou, M. Han, P. Wang, Rheological behavior, conformational changes and interactions of water-soluble myofibrillar protein during heating, *Food Hydrocoll.* 77 (2018) 524–533, <https://doi.org/10.1016/j.foodhyd.2017.10.030>.
- [33] M.H. Lee, H. In Yong, Y.J. Kim, Y.S. Choi, High-pressure induced structural modification of porcine myofibrillar protein and its relation to rheological and emulsifying properties, *Meat Sci.* 196 (2023), 109032, <https://doi.org/10.1016/j.meatsci.2022.109032>.
- [34] T.K. Kim, M.H. Lee, H.I. Yong, M.C. Kang, S. Jung, Y.S. Choi, Porcine myofibrillar protein gel with edible insect protein: effect of pH-shifting, *LWT* 154 (2022), 112629, <https://doi.org/10.1016/j.lwt.2021.112629>.
- [35] A. Amiri, P. Sharifian, N. Soltanizadeh, Application of ultrasound treatment for improving the physicochemical, functional and rheological properties of myofibrillar proteins, *Int. J. Biol. Macromol.* 111 (2018) 139–147, <https://doi.org/10.1016/j.ijbiomac.2017.12.167>.
- [36] K. Li, Z.L. Kang, Y.Y. Zhao, X.L. Xu, G.H. Zhou, Use of high-intensity ultrasound to improve functional properties of batter suspensions prepared from PSE-like chicken breast meat, *Food Bioprocess Technol.* 7 (2014) 3466–3477.
- [37] K. Xu, C. Wu, G. Fan, X. Kou, X. Li, T. Li, J. Dou, Y. Zhou, Rheological properties, gel properties and 3D printing performance of soy protein isolate gel inks added with different types of apricot polysaccharides, *Int. J. Biol. Macromol.* 242 (2023), 124624, <https://doi.org/10.1016/j.ijbiomac.2023.124624>.
- [38] X. Ran, H. Yang, Promoted strain-hardening and crystallinity of a soy protein-konjac glucomannan complex gel by konjac glucomannan, *Food Hydrocoll.* 133 (2022), 107959, <https://doi.org/10.1016/j.foodhyd.2022.107959>.
- [39] Z. Li, J. Wang, B. Zheng, Z. Guo, Impact of combined ultrasound-microwave treatment on structural and functional properties of golden threadfin bream (*Nemipterus virgatus*) myofibrillar proteins and hydrolysates, *Ultrason. Sonochem.* 65 (2020), 105063, <https://doi.org/10.1016/j.ultsonch.2020.105063>.
- [40] D.C. Kang, Y.H. Zou, Y.P. Cheng, L.J. Xing, G.H. Zhou, W.G. Zhang, Effects of power ultrasound on oxidation and structure of beef proteins during curing processing, *Ultrason. Sonochem.* 33 (2016) 47–53, <https://doi.org/10.1016/j.ultsonch.2016.04.024>.
- [41] H. Shi, X. Zhang, X. Chen, R. Fang, Y. Zou, D. Wang, W. Xu, How ultrasound combined with potassium alginate marination tenderizes old chicken breast meat: possible mechanisms from tissue to protein, *Food Chem.* 328 (2020), 127144, <https://doi.org/10.1016/j.foodchem.2020.127144>.
- [42] X. Wang, M. Xia, Y. Zhou, L. Wang, X. Feng, K. Yang, J. Ma, Z. Li, L. Wang, W. Sun, Gel properties of myofibrillar proteins heated at different heating rates under a low-frequency magnetic field, *Food Chem.* 321 (2020), 126728, <https://doi.org/10.1016/j.foodchem.2020.126728>.
- [43] X. Gao, J. Yongsawatdigul, R. Wu, J. You, S. Xiong, H. Du, R. Liu, Effect of ultrasound pre-treatment modes on gelation properties of silver carp surimi, *LWT* 150 (2021), 111945, <https://doi.org/10.1016/j.lwt.2021.111945>.
- [44] Y. Li, S. Zhang, Z. Bao, N. Sun, S. Lin, Exploring the activation mechanism of alkalase activity with pulsed electric field treatment: effects on enzyme activity, spatial conformation, molecular dynamics simulation and molecular docking parameters, *Innovative Food Sci. Emerg. Technol.* 76 (2022), 102918, <https://doi.org/10.1016/j.ifset.2022.102918>.
- [45] N. Baildya, N.N. Ghosh, A.P. Chattopadhyay, Inhibitory activity of hydroxychloroquine on COVID-19 main protease: An insight from MD-simulation studies, *J. Mol. Struct.* 1219 (2020), 128595, <https://doi.org/10.1016/j.molstruc.2020.128595>.